Risø-R-1374(EN)

Design of a 21 m Blade with Risø-A1 Airfoils for Active Stall Controlled Wind Turbines

Peter Fuglsang, Risø National Laboratory
Ole Sangill, Norwin A/S
Peter Hansen, LM Glasfiber A/S

Risø National Laboratory, Roskilde
December 2002

Abstract
This is the final report, from the project, "Design of a Rotor/Airfoil Family for Active Stall-regulated Wind Turbines by Use of Multi-point Optimization". It describes the full scale testing of a 21 m wind turbine blade specially designed for active stall regulation. Design objectives were increased ratio of produced energy to turbine loads and more stable power control characteristics. Both were taken directly into account during the design of the blade using numerical optimization. The blade used the Risø-A1 airfoil family, which was specially designed for operation on wind turbine blades.

The new blade was designed to replace the LM 21.0P blade. A measurement campaign was carried out simultaneously on two identical adjacent wind turbines where one had the new blades and the other had LM 21.0P blades. Power and loads including blade section moments for the new blades were measured to assess the characteristics of the new blade. Airfoil characteristics, power curve and fatigue loads were derived on basis of the measurements.

Most of the design criteria for the new blade were met. The new blade had a reduced weight of 4% reducing blade cost compared with LM 21.0P. The measurements showed that the wind turbine with the new blades had the same energy production as the wind turbine with LM 21.0P blades but at the same time a 15% decrease in blade fatigue loads. However, the derived airfoil characteristics for the new blade were not in good agreement with the expected characteristics. The new blade was more sensitive to roughness and imperfections at the leading edge than initially foreseen and a high relative thickness in the tip region caused an unexpected drop in the maximum lift coefficient. This lead to discrepancies between the initial expected and actual pitch control characteristics.

It could be concluded that the new LM 21.0 ASR blade could replace the LM 21.0P leading to improved cost efficiency and that the Risø-A1 airfoils were well suited for active stall control. With the new established knowledge of the actual airfoil characteristics, a possible future blade design could be made also with improved power control characteristics.

The project was partially funded by the Danish Energy Agency under the contract, UVE-J.nr.51171/99-0028.

The project consortium involved LM Glasfiber A/S, WEA Technology A/S, Norwin A/S and Risø National Laboratory with the following responsible persons:

- Per Lading, WEA Technology, responsible for the measuring campaign.
- Troels Eske Nielsen, Risø National Laboratory, made the power curve analysis.
- Peter Fuglsang, Risø National Laboratory, responsible for part A "Derivation of airfoil coefficients for NW46 with LM 21.0 ASR blades"
- Ole Sangill, Norwin A/S, is responsible for part B "Power-curve and load assessment of LM 21.0 ASR blades", and for the project coordination.

ISBN 87-550-3137-4
ISBN 87-550-3138-2(Internet)
ISSN 0106-2840

Print: Pitney Bowes Management Services Danmark A/S, 2002

Contents

1 Introduction

Design of wind turbine blades with special purpose airfoils has been a target for intensive research for many years. In 1998 the aeroelastic design research programme of the wind energy department at Risø National Laboratory had come so far in this research that not only was it thought that the properties of a wind turbine blade could be predicted with sufficient accuracy, but additional design tools had been developed making it possible to optimize the blade for a specific purposes, i.e. a special turbine regulation strategy.

WEA has since 1994 developed wind turbines with Active Stall Regulation (ASR) with the first prototype erected in 1995. In 1997 cooperation and further development work was started together with Norwin.

From the very beginning of the turbine development work it was clear that the optimal performance for active stall regulation could not be reached using traditional blades designed for passive stall or pitch regulation. To make a better product it would be necessary to integrate the blade design in the development of the entire turbine including power control. This is a fact for all types of modern wind turbines using active regulation to improve performance, and it has become the trend in today's wind turbine development.

The straightforward idea that initiated this project was to combine the needs in the industry, - to optimize the cost-effectiveness of wind turbines using more advanced types of regulation systems -, with the available research results and tools for designing a specific purpose blade.

The general project objective was to design and test a blade with improved qualities compared to traditional blades. One of the important design constrains was the turbine control system. The work approach was to conduct a theoretical design study followed by a practical test that should be carried out if the design study showed promising results. The evaluation was based on measurements on full-scale test blades mounted on a Norwin 46-ASR-600 kW (NW46) wind turbine. For comparison, measurements were taken simultaneously on a similar neighbor turbine mounted with traditional blades.

Since the entire concept needed investigation and the design parameters needed to be defined first, the project was separated in two phases:

1. Definition of design parameters, outline of the initial new aerodynamic blade design and evaluation of the achieved benefits on a theoretical basis.
2. Aerodynamic and structural design of a blade, manufacture, approval and installation of the blade to measure performance and evaluate results.

The conduction of Phase 1 was finalized in August 99, with promising results [1]. It was therefore decided to continue with Phase 2. This report describes this test and evaluation phase, focusing on expectations and results. Chapter 2 outlines a short repetition of the expectations and findings from phase 1 and discusses the initial criteria for success for the entire project work. Chapter 3 gives a description of the work and an assessment of the results. Finally, an evaluation of the criteria of success and a conclusion was made for the whole project work in chapter 4.

In the main part of the report, chapter 1 to 4, a lot of interesting technical details was left out. Some of these details may be found in the appendices. Appendix A describes how airfoil coefficients were derived for the LM 21.0 ASR blades mounted on the NW46 wind turbine. Chapter B shows the details of the power curve and load assessment on the blade.

2 Criteria for success

Active stall regulation (ASR) is the term for regulation of a wind turbine, using the stall properties of the blades to limit the power output at high wind speeds. The blades are pitched into stall, in contrast to traditional pitch regulation where the blades are pitched out of stall. Continuous featherings of the blades are used to optimize the power output at low wind speeds, to control the power output at high wind, and during breaking and parking.

The specific objective of this project was to develop a 21m-blade optimized for wind turbines with ASR, in the sense that it would be more cost effective, have more stable properties, and have a lower production price compared to a 'state of the art' blade designed for traditional stall regulated wind turbine. Increased cost effectiveness means an increased ratio of produced energy to loads on the turbine.

The work in project Phase 1 was concentrated on defining design parameters, outlining the initial new aerodynamic blade design and finally evaluating the achieved benefits on a theoretical basis. The evaluation of the new blade was compared to the LM 21.0 P blade, which currently is used with good results on the NW46 turbine. Investigations and findings from Phase 1 were reported in [1] and is shortly summarized in the following.

For the new ASR blade and the traditional LM 21.0P blade to be comparable it was decided that the blade length and the root diameter should remain unchanged. To avoid a change in the structural turbine response that could make the interpretation of loads difficult it was decided to keep the natural frequencies for the new ASR blade as close to the LM 21.0 P blade as possible.

The first set of design/optimization parameters were found through an analysis of the ASR regulation leading to a description of how the blade should be designed to best suit the regulation purpose. An aerodynamic analysis was made with the Norwin 46 turbine as basis. This defined the primary demands to the airfoils and the blade to obtain maximum energy output without violating the demands from the ASR regulation. As a consequence of the investigations conducted the airfoils for the blade could be chosen. It was decided to use the Risø-A1 airfoil family as basis. These airfoils had for the given task seemingly better properties compared to the NACA 63-4xx profile series on LM 21.0P. Furthermore, three of the Risø-A1 airfoils were verified in wind tunnel measurements [11].

Having defined the main design parameters, the blade optimization could take place, utilizing the numerical optimizations program HAWTOPT [6]. This optimization tool is using cost functions to find the change in turbine costs from changes in the loading on the turbine. A cost function complex had been developed for the Norwin 46 turbine. It was for convenience decided not to use the cost functions for the blades during the optimization process. The entire design complex was used only in the final evaluation process. The design process involved using the aero-elastic model in FLEX4 [5] of Norwin 46 including ASR regulation. To avoid confusion between blade and regulation properties it was decided to apply the simplest available ASR regulation strategy.

As an addition to the requirements for the new blade it was decided that it should be approximately 3 percent points thicker than the LM 21.0P blade. This would make the blade relatively stiffer, which was estimated to reduce blade costs, especially for future blades in the multi MW class. The tip region of the blade was kept equal to the tip of LM 21.0P to avoid changes with respect to noise and tip properties in general. A significant result from the optimization was that the chord distribution was chosen so that the blade would be 6% more narrow leading to a 6% reduction in area compared with LM 21.0P. This was made possible because the Risø-A1 airfoils have a higher design lift coefficient than the traditional NACA airfoils on the LM 21.0P blade.

The FLEX4 model of the Norwin 46 wind turbine was used to calculate Aero-elastic loads and energy production. The complete cost function was applied on the turbine operating with the traditional LM 21.0 P blade and the new LM 21.0 ASR blade. The result was that a wind turbine with the optimized LM 21.0 ASR blades had an energy output increase of 2.75% compared to the traditional LM 21.0P blade, with a

decrease in blade price at the same time. The extreme loads on the turbine was distributed slightly differently, but was in general a little bit lower mainly due to the decrease in blade area, while the fatigue loads showed a general increase in the order of 1-2%. Collectively evaluated, the new blade was more cost effective than the traditional blade. Added to this was a number of other qualities such as the improved ASR regulation properties of the new blade. Furthermore, the increased blade thickness resulted in a 6% lighter blade which evaluated on a 50 m blade would result in a weight decrease of 8.5% compared to traditional designs.

Concluding on the theoretical results for the new LM 21.0 ASR blade design, it had reached the target for project Phase 1:

- Improved cost efficiency.
- Improved controllability and decreased weight.

It was therefore decided to continue with the full-scale test of the new blade on a Norwin 46-ASR-600 kW wind turbine.

To assess if the accomplishments from the full-scale tests were in line with the theoretical estimates, the criteria for success for the tests and the general project results could be outlined. (Table 2-1):

Table 2-1 Criteria for success for the design of the new ASR blade.

Type of blade property:	**Criteria's for success:**
1. Structural properties:	A lighter blade A lower cost blade
2. Airfoil data:	A good agreement between measured and theoretical airfoil data Insensitivity to roughness
3. Power curve:	Increased energy output to load ratio
4. Loads:	Decreased load to energy output ratio
5. Control characteristics:	Less demand for pitch activity Higher tolerance to pitch errors (less power overshoot)

3 Assessment of results for LM 21.0 ASR

3.1 Structural properties

The LM 21.0 ASR blade was build as a modified version of the LM 21.0 P blade. The main differences were airfoil choice, rotor solidity and relative thickness. As stated in chapter 2, the aim was to be able to reduce loads by reducing the rotor solidity, keep the power production by selecting airfoils with higher design lift and reduce weight by increasing the relative thickness of the airfoils.

Figure 3-1 and 3-2 compare the LM 21.0 ASR blade with the LM 21.0 P blade.

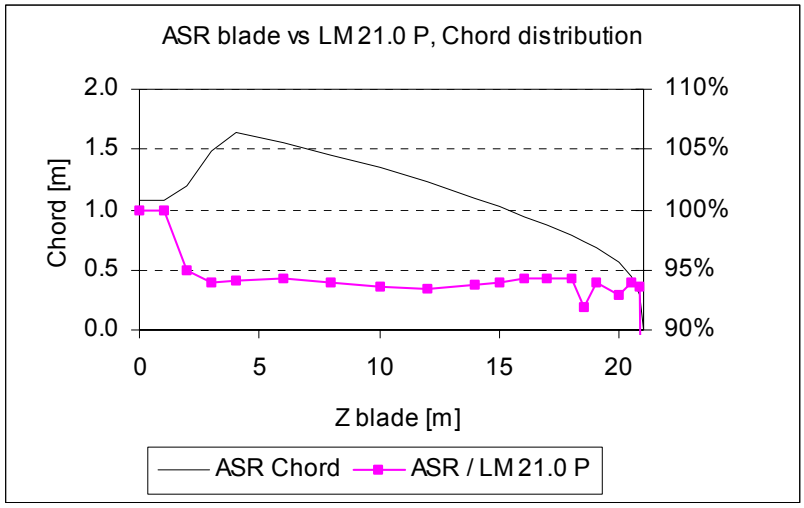

Figure 3-1 Blade chord (left axis), and relation in percentage (right axis), between the LM 21.0 ASR and the LM 21.0 P blade, as function of blade length.

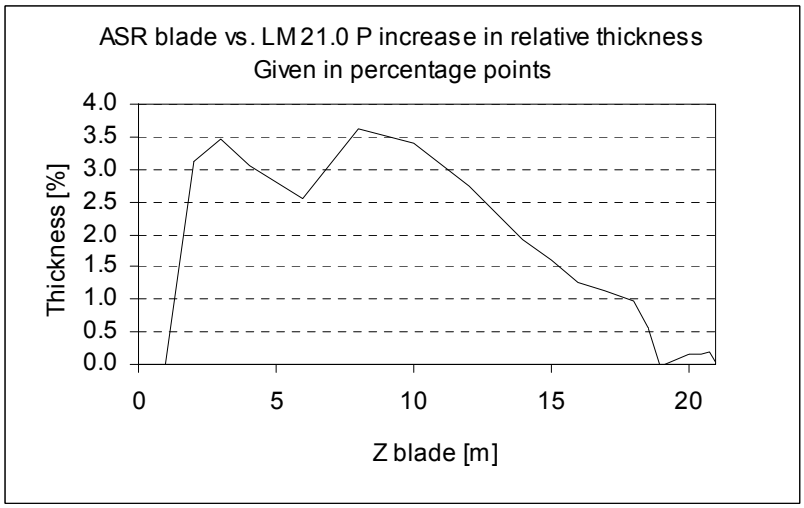

Figure 3-2 The relative increase in thickness for the LM 21.0 ASR blade compared to the LM 21.0 P blade, as function of the blade length.

The increase in relative thickness for LM 21.0 ASR resulted in a small increase in absolute thickness in spite of the smaller chord. This allowed the flapwise strength and stiffness to be maintained with a lower weight over the major blade length. However, as a consequence of the smaller chord the edgewise

frequency was decreased. Too keep the frequency within a desired level not too far from the LM 21.0 P blade a reinforcement of the structure in the edgewise direction was necessary. This reinforcement was made between 4 m and 9 m span, and resulted in an increase in blade mass of 40 kg.

Table 3-1 shows the natural frequencies of the blades. A reduction of the flapwise stiffness was allowed, since the reduction in blade area gave a reduction of loads and extreme deflection.

Table 3-1 Blade natural frequencies.

Blade type:	LM 21.0 P	LM 21.0 ASR
Frequency:	[Hz]	[Hz]
1. Flapwise bending	1.58	1.46
2. Flapwise bending	4.94	4.16
1. Edgewise bending	3.44	3.05

Table 3-2 Measured blade mass.

Blade type:	LM 21.0 P	LM 21.0 ASR	LM 21.0 ASR no reinforcement
Blade mass [kg]:	2110	2065	2025
Relation to LM 21.0 P:	1.00	0.98	0.96

Table 3-2 shows the measured blade mass. For the prospects of the new blade design, the weight of the LM 21.0 ASR blade without reinforcement was the most interesting because this was how the blade would have been made, if the natural frequency constraint had not been forced on the design. It was found that a weight decrease of approximately 4% could be expected with a blade of this size. This was a little less than the expected decrease of 6% found in the project Phase 1. Still it was a good achievement that for a 50 m blade would give a weight decrease of approximately 5.5 %. Consequently, the new blade design would at the same time be app. 4% lighter, resulting in a decrease in the edgewise bending fatigue loading (which normally is dimensioning the blade root section), and app. 4% cheaper to manufacture assuming that price is proportional to the weight.

3.2 Airfoil data

The airfoil coefficients were derived for the LM 21.0 ASR blades mounted on the NW46 wind turbine on basis of measurements of generator power and selected blade section moments. A systematic method based on numerical optimization and an aero-elastic code was used for adjusting the airfoil coefficients along the blade so that predicted values of power and section moments became in agreement with measurements. Solving a problem like this is not trivial because of the high number of possible solutions and the results will always be associated with uncertainty. The reliability of the resulting airfoil coefficients was assessed by comparison with 2D wind tunnel results for relevant airfoil sections and by analyzing the operation of the NW 46 wind turbine using FLEX4.

An analysis of the measurements showed that the measured generator power was in good agreement with the initial design target at low wind speeds whereas at high wind speeds the initial design target was overestimating power compared with the actual measurements. On the contrary the measured blade flapwise section moments were lower than the initial design prediction.

The generator power and the blade flapwise section moment at rotor radius 2.7 m were found reliable and usable. This was considered to be an absolute minimum for reliable determination of airfoil coefficients.

The LM 21.0ASR blade was divided into three parts:
(1) The blade tip with the Risø-A1-15 airfoil from rotor radius 20 m to 23 m.
(2) The blade outer part with Risø-A1 (18% to 24%) where one compound airfoil characteristic represented the region from 12 m until 20m.

(3) The blade root part from 0 m to 12 m where the initial guess on the airfoil characteristics were used.

Airfoil coefficients were determined for part (1) and (2) resulting in a near perfect match between measured and predicted generator power and good agreement between measured and predicted blade root flapwise moments. The resulting airfoil coefficients for the tip region (1) showed a maximum c_l slightly lower than the initial guess, which corresponded closely to 2D measurements. This was in agreement with the general trends for 3D rotor aerodynamics in [2]. The resulting airfoil coefficients for the blade outer part (2) showed a maximum c_l, which was somewhat, lower than expected. A comparison of the derived airfoil coefficients with 2D wind tunnel measurements suggested that measurements with leading edge roughness should be used for this part of the blade.

The main reason for the discrepancy between the initial design prediction of generator power and the actual measurements were addressed to the different performance of the blade outer part. Possible explanations were:

- The Risø-A1 airfoils are more sensitive to roughness than initially foreseen.
- The LM 21.0ASR blade had imperfections in the leading edge region, which lead to poorer aerodynamic performance than expected.
- The high relative thickness of the LM 21.0 blade caused a drop in aerodynamic performance because of a difference in the actual 3D airfoil data compared with the 2D wind tunnel data for airfoils of high relative thickness.

For future blade designs two general guidelines could be established:

- Sensitivity to leading edge roughness and imperfections in the leading edge region for the outer half of the blade should be taken into account by use of less optimistic airfoil data.
- The relative thickness of the outer part of the blade should be chosen with great care. A high relative thickness should only be chosen when necessary from a structural viewpoint or when the blade flapwise loads should be minimum.

Despite the unforeseen difference in the initial guess on the airfoil data and the actual derived airfoil coefficients the measurements showed good results for the annual energy yield and low flapwise loads at high wind speeds.

Appendix A shows the derivation of airfoil characteristics in more detail.

3.3 Power curve

The power curve measurements took place for a period of approximately a year, with the results successively evaluated. To be able to compare LM 21.0 ASR with LM 21.0P, measurements were conducted simultaneously on two adjacent Norwin 46-ASR-600 kW wind turbines; Ørsted 2 equipped with traditional LM 21.0 P blades, and Ørsted 1 equipped with the new LM 21.0 ASR blades.

During the blade comparison measurement period the turbines were running with the most simple type of blade regulation, where the blade angle pitch setting was defined according to a fixed table linking wind speed and pitch angle. The reason for this choice was firstly that it would make the analysis of the measuring results much easier than if the turbine would regulate itself according to a complex procedure. Secondly, that the results could be published without restrictions because the simple regulation method is not considered as critical knowledge. A number of tests and adjustments to optimize the pitch angle settings were conducted before commencing the actual power curve measurements.

Figure 3-3 shows the results of the measurements. It was found that the power performance for the two turbines were fairly similar, with a tendency that the power curve for the turbine with the new LM 21.0 ASR was slightly better, except for the wind speed range from 12 m/s to 14 m/s (explained in Appendix A). This was in correspondence with the operational experience from the turbine, where it was found that the energy output from the two turbines was almost the same. It was generally assessed that the performance from the turbines should be rated to be equal.

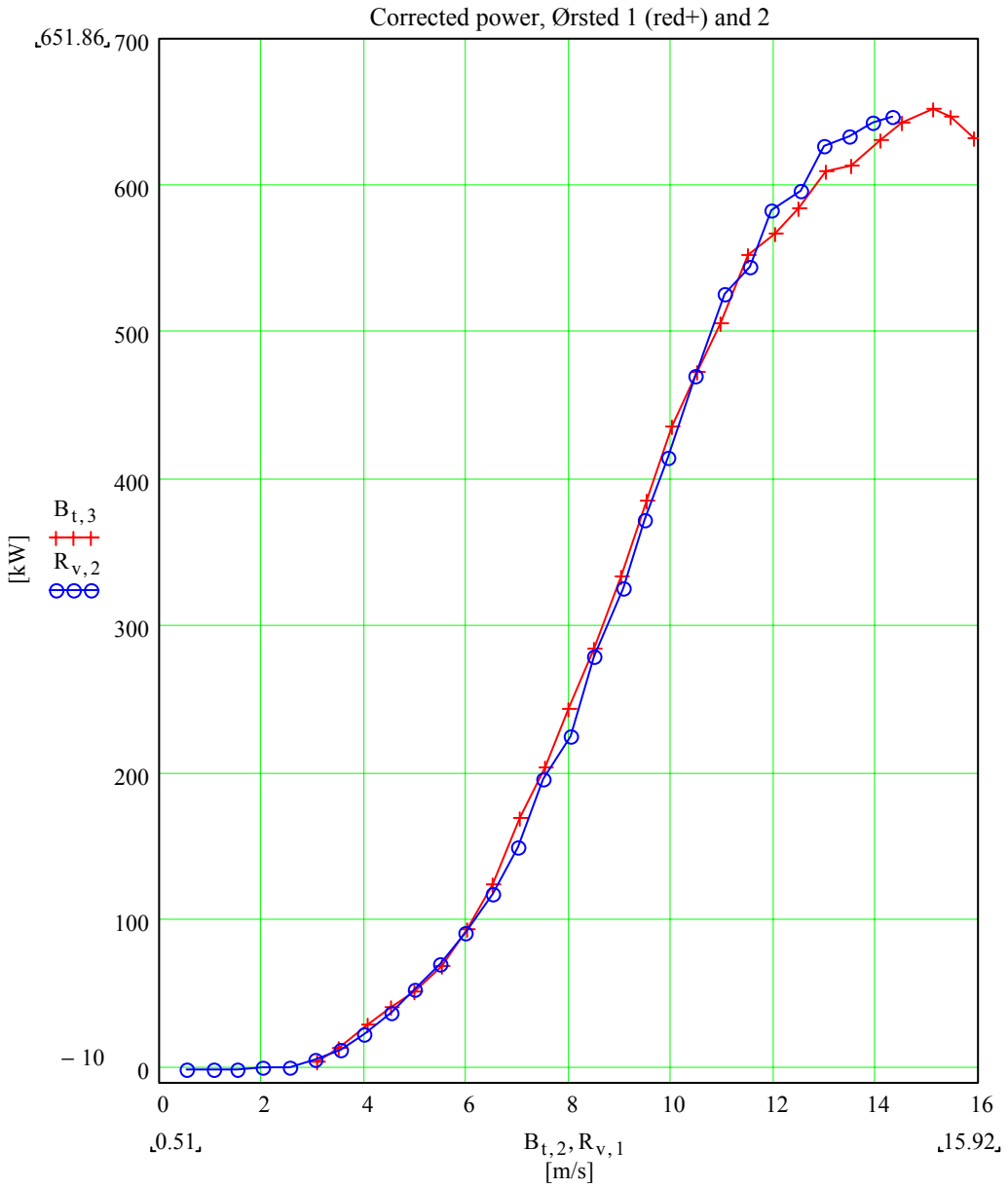

Figure 3-3 Power curve for the Norwin 46 turbine with LM 21.0 ASR blades compared with LM 21.0 ASR blades shown as binned values, corrected to air density 1.225 kg/m^3.

3.4 Loads

The load measurements took place over a period of approximately half a year. While the evaluation process for the power performance was a fairly straightforward analysis of the statistical data, the load evaluation process was more complicated, because the statistical derivatives of the measured quantities were not the result of most significance. Seen in perspective of the turbine running in the normal operating range, the most important figures to evaluate were the fatigue loads. The strategy for the analysis of loads was to follow a two-step process:

1. To prove that the loads simulated with FLEX4, using the derived airfoil coefficients and the measured turbulence and air density, gave the same results as the measured loads.
2. To compare energy output and loads between the new LM 21.0 ASR blade and the traditional LM 21.0P blade by means of simulation. It would have been preferred to compare measurements to measurements directly, instead of using simulations, but since blade measurements were not made on the traditional blades this was unfortunately not an option.

The analysis of the measured data was conducted on a representative time series sampled with 40 Hz, with a total duration of 142.5 hours. Represented wind speeds ranged from 3 m/s to 18 m/s, sliced into time series of 5 minutes. To calculate the fatigue damage loading, in terms of a load range table, a rain flow counting procedure was applied on each time series. To be able to express the result from each time series as a single value the load range table was recalculated into an equivalent load range (S/N curve slope m=8). Calculating also the average wind speed for each time series, the result of the analysis so far was that each time series was represented by two figures: An average wind speed and an equivalent load range value. Since it would be convenient for the comparison later on to be able to represent the result from all the time series as a curve of equivalent load range as function of wind speed, a binning procedure was used (again with S/N curve slope m=8), recalculating the equivalent load ranges within predefined wind speed ranges to a single value.

To compare measured and simulated results, a number of time series were simulated with FLEX4 for the wind speeds in the investigated range, using the measured turbulence and air density as input parameters. Then following the exact same analysis procedure as were used on the measured data, figures connecting average wind speed and equivalent load ranges could be established for the simulated data. Measured and simulated data were then directly comparable, since they were in the same format, and derived in exactly the same manner. Making the comparison for the measured quantities, the most convincing result was found for the flapwise blade bending shown in Figure 3-4, where the measured and calculated loads are in excellent agreement in the entire wind speed range.

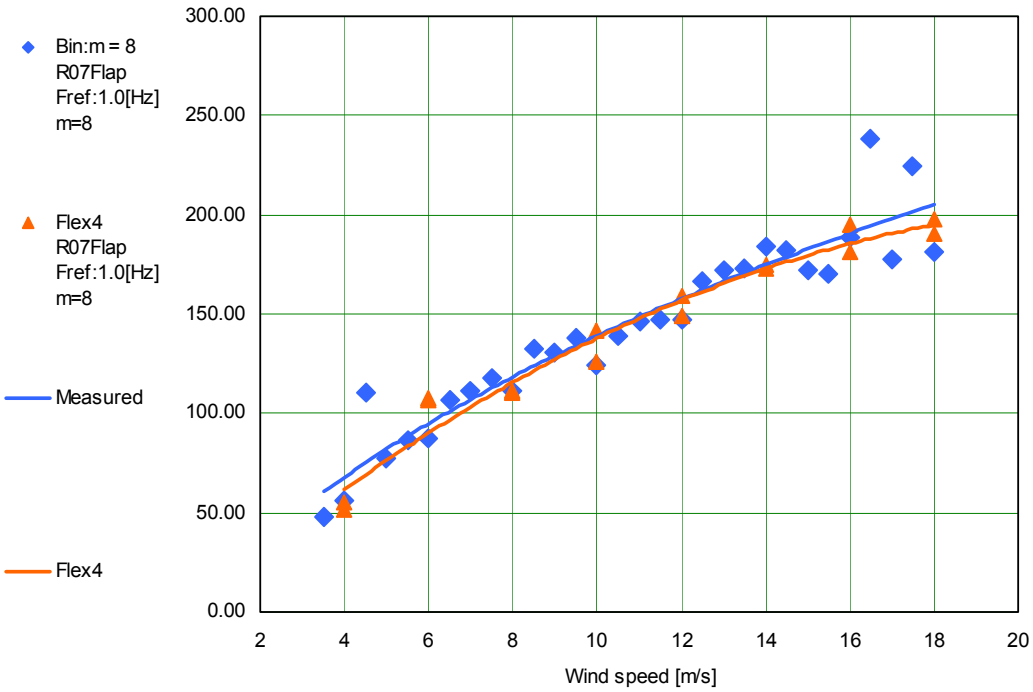

Figure 3-4 Equivalent load of flapwise blade bending in radius 0.7 m from blade root as function of wind speed shown as bin values from measurements and points calculated with FLEX under the same wind and air density conditions. Calculated and binned for S/N-curve exponent value m=8 (1Hz load cycle frequency).

Having established that the measured and calculated loads for the LM 21.0 ASR blade were in good agreement, made it possible to compare the loads between the new and the traditional blades on a calculation basis. The comparison was made for the turbine running in 20 years of operation in the wind speed range from 4 m/s to 18 m/s. The fatigue loads were calculated for each of the sensors: Electrical power (Power1), flapwise bending (R1Flap), edgewise bending (R1Edge) and power load density distribution equivalence (Power1ldd), expressed as a single value for the equivalent load range. The

power load density distribution equivalence indicated the resulting load on the gearbox and was derived directly from the power, using the proportionality between power and main shaft torque.

Since a load change could be balanced out by a likewise change in the energy production from the turbine, a comparison of the loads alone would not be sufficient for the evaluation process. To get a complete picture it was necessary to compare the energy output to load ratio, and for this reason the energy production during the 20 years of operational period was calculated from the simulations as well.

For the operational conditions in the period two types of terrain was looked at: A standard terrain type with a high average wind speed, and a terrain type 2 with a medium wind speed (the same as were used in [1]). As before a S/N curve slope of m=8 was used for the fatigue calculation.

Three blade designs were looked at. First the original LM 21.0 P blade, second the new blade using the airfoil data as they were assumed to be after phase 1 of the project and third the new blade using the airfoil data derived from the measurements. In the simulation the full power level regulation was used in order to include aspects of the blades regulation properties into the analysis. The calculation of the LM 21.0 P blades was based on the airfoil data provided by LM Glasfiber.

Table 3-3 shows the results of the calculations. To make the evaluation easier the derived values were expressed as percentage of load and energy production for the traditional LM 21.0 P blade.

Table 3-3 The calculated fatigue load and corresponding energy yield, for the turbine operating between 4 m/s and 18 m/s for a site with high average wind speed and a site with medium average wind speed. The result shown is a comparison between the LM 21.0 P blade and the LM 21.0 ASR blade with two different estimates of the airfoil coefficients (the estimate after phase 1 of the project, and the final estimate based on the load assessments). The comparison is in percentage of the figures for the LM 21.0 P blade.

Total operating fatigue loads and energy yield
Base: N=10E7 m=8
Standard terrain type (High wind regime)
Comparison to LM21.0P in percentage

	LM210P Blade	Phase1 ASR blade	Final ASR blade
Power1	100	101	87
R1Flap	100	94	77
R1Edge	100	98	91
Power1ldd	100	104	99
Energy	100	103	100

Total operating fatigue loads and energy yield
Base: N=10E7 m=8
Terrain type 2 (Medium wind regime)
Comparison to LM21.0P in percentage

	LM210P Blade	Phase1 ASR blade	Final ASR blade
Power1	100	102	87
R1Flap	100	94	77
R1Edge	100	98	93
Power1ldd	100	104	98
Energy	100	103	100

Focusing on the traditional LM 21.0 P blade and the Final LM 21.0 ASR blade, it was found that the energy yield from the blades were the same, which was supported by the analysis of measured power of the two turbines during the testing period. It was expected after end of project Phase 1 [1] that the blades would produce approximately 3% more energy, but this showed not to be the case.

With equal energy production from the blades, the loads could be compared directly, and here a significant difference was found. After project Phase 1 [1] the loads were expected on average to increase slightly. Looking at the results for the Final LM 21.0 ASR blade it was seen that the loads on the contrary were decreased significantly. The blade loads were decreased with approximately 15% in average, and the power load (i.e. applied to main shaft torque) was decreased with approximately 13%. The power load density distribution equivalence was only slightly decreased which was expected since it is tightly linked to the produced energy.

3.5 Control characteristics

To have an ideal pitch curve, as outlined in [1], the curve profile should be a monotonous decrease with wind speed in the wind speed region from 4 m/s to 12 m/s and then be horizontal flat in the entire stall range. As shown in Figure 3-5 an attempt to design the blade accordingly was made. Note that the practical curve would be smoothened out between 3 m/s and 13 m/s. The obtained (measured) pitch curve was also shown in Figure 3-5 and it did obviously not have this quality. The main reason for this was the discrepancy between the initial predicted airfoil characteristics and the actual airfoil characteristics. The actually obtained Cl_{max} was somewhat lower than anticipated, and it was therefore necessary to increase the pitch angle by up to 2 degrees more than anticipated to match the initially predicted power curve.

A pitch characteristic like the measurement in Figure 3-5 means that more pitch action is demanded to control the turbine power output. An increased fatigue load on the pitch system is therefore unavoidable. However, it also means a higher number of situations where the pitch angle is incorrectly adjusted with respect to wind speed and resulting power level. From this it could be expected that the standard deviation of the power was higher for the LM 21.0 ASR blade compared with the LM 21.0P blade where the pitch characteristic is much closer to the ideal case. Both the daily turbine operation and the measured loads showed that this was not the case, which in terms showed that the blades had a less violent response to adjustment errors, and thus less load penalty.

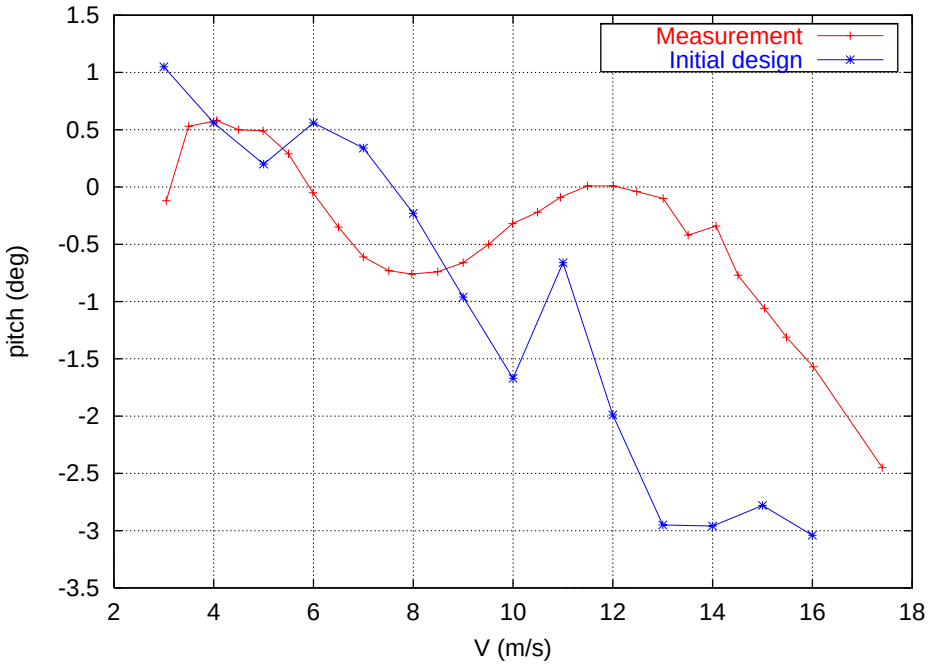

Figure 3-5 Pitch angle versus wind speed.

Summing up on the results, less demand for pitch activity was not obtained. However, in spite of increased pitch activity, and increased chance of adjustment errors, the final results of the load analysis on the power signal showed a general decrease in blade fatigue loading, as shown in 3.4, indicating that the blade design had a higher tolerance to pitch errors.

4 Conclusion

The project objective was to design and test a specific purpose blade for active stall control with improved qualities compared to a traditional blade. The idea was to combine the needs in the industry; for optimizing the cost-effectiveness of wind turbines using more advanced types of regulation systems, with the latest available research results and tools for airfoil and blade design so that the control strategy for the turbine was actually taken into consideration in the blade development process.

In the theoretical development phase of the project it was shown to be possible to design a blade featuring specially designed airfoils that in addition to the improved control characteristics would have a number of other advantageous properties like lower weight and increased cost-effectiveness.

The target of the full-scale test phase of the project was to evaluate if these properties were actually obtainable in reality. To validate the results a set of criteria for success for the properties of the new blade was established. In the following each of those were addressed based on the results from the full-scale testing of the new blade:

Property:	**Criteria's for success:**	**Rating:**	**Comment:**
Structure:	A lighter blade	☺	Blade mass decreased by 4%
	A lower cost blade	☺	Blade price decreased by 4%
Airfoils:	Agreement between measured and theoretical airfoil data	😐	Some airfoils, especially those between 18% and 24% relative thickness were in less good agreement
	Insensitivity to roughness	😐	The blades was more sensitive to roughness than initially foreseen
Power:	Increased energy output to load ratio	☺	The energy output was maintained, but the loads were decreased (in simulations)
Loads:	Decreased load to energy output ratio	☺☺	The blade loads are i.e. decreased with app. 15% while maintaining energy output (in simulations)
Control:	Less demand for pitch activity	☹	The target pitch curve was not met
	Higher tolerance to pitch errors (less power overshoot)	☺	The result indicated higher tolerance

Not all success criteria were met. This was mainly because of the discrepancy between estimated and actual airfoil characteristics. For the outer part of the blade the resulting airfoil coefficients were not in good agreement with the initial guess, which was used for the design of the blade. The actual maximum lift coefficient was lower than expected for the airfoils between 18% and 24% relative thickness. This explained the difference in the measured pitch-regulation curve compared with the initial design pitch-regulation curve. The results indicated that sensitivity to roughness and imperfections at the leading edge together with the high relative thickness of the outer part of the LM 21.0ASR blade caused a poorer aerodynamic performance than what was expected during the initial design.

Most of the design criteria were met with better results than initially expected. It was possible to make a specific purpose blade for active stall control with specially designed airfoils. The blade weight was reduced leading to a reduction in production costs. Compared to the reference blade, LM 21.0P, the annual energy output was the same but at the same time the loads were significantly reduced.

It could be concluded that the new LM 21.0 ASR blade could replace the LM 21.0P leading to improved cost efficiency and that the Risø-A1 airfoils were well suited for active stall control. With the established knowledge of the actual airfoil characteristics, a possible future blade design could be made also with improved power control characteristics.

A Derivation of airfoil coefficients for NW46 with LM 21.0 ASR blades

A.1 Introduction

When blade element momentum theory is used to calculate power and loads, it is necessary to adjust the two-dimensional airfoil coefficients to achieve correct results. The adjustments compensate for the simplifications that form the basis for this relative simple theory such as the two-dimensional flow in annular stream tubes. With some experience it is possible to get good agreement between calculated and measured power by manually adjusting the airfoil c_l and c_d curves [2]. There is only little guidance in the literature on how the airfoil coefficients are affected by three-dimensional flow, e.g., in [3] and [4].

It is difficult at the same time to get agreement between measured and calculated loads. The power and also the blade bending moments are integral quantities, that do not in themselves contain information about the load distribution on the blades and therefore the determination of the correct blade force distribution is problematic. To achieve the correct force distribution it is necessary to compare calculations of both power and multiple blade section moments with measurements. This is a complex inverse problem, which can only be solved manually with difficulty. This chapter describes how a systematic method was applied to find suitable airfoil characteristics for the NW46 wind turbine with LM 21.0ASR blades.

The method applied systematic numerical optimization, where adjusting the airfoil coefficients in an iterative process minimized the error between measurements and calculations. This enabled agreement between measurements and calculations for mean values versus wind speed of power and loads.

A.2 Method

The inverse problem of determining airfoil coefficients from measurements by use of this method consists of the following items:

1. Measurements of power and loads under normal operation.
2. An aeroelastic model of the wind turbine structure including the rotor.
3. An aeroelastic code coupled to an optimization algorithm.
4. An initial guess on the airfoil coefficients (c_l and c_d).

A.2.1 Measurements

The measurements should cover normal operation in as large a wind speed interval as possible. To improve the statistical certainty, the measurements should be averaged into 10-minute values. Measurements at large yaw error or other non-typical operation conditions should be excluded. A mean value curve should be processed for each measured quantity by sorting the measurements into wind speed bins covering the wind speed operation interval.

A.2.2 Aeroelastic code

An aeroelastic code was used to calculate power and loads. In this work the FLEX4 code was used [5].

The calculations were compared to averaged measurements in wind speed bins. Therefore, the wind field was uniform without turbulence. The time series length should cover several rotor rotations to eliminate the periodicity of power and loads with rotor azimuth. In this case 30-second time series was used for each wind speed end eventual transients in the beginning of each time series were removed.

Even proper calculation of mean loads requires a valid aeroelastic model of the wind turbine. The aeroelastic model of the wind turbine should include all relevant degrees of freedom so that the conditions for the calculated loads are equal to the measurement conditions. For example the calculation of blade section moments should include the centrifugal stiffening of the blades. Furthermore the gearbox, generator and the power control should be modeled properly.

A.2.3 Numerical optimization

FLEX4 was coupled to the Risø design tool, HAWTOPT [6] [7]. In general terms the optimization problem consists of the objective function, f and the design variables in the design vector, **x**. Furthermore the constraints, **g**, can bound both design variables and calculated response parameters. The design variables are changed so that f is minimized.

In this work the objective function, f, was calculated as a root mean squared sum:

$$f = \sum_j w_2 \sum_i \sqrt{w_{1_{i,j}} \left(L_m - L_c\right)^2_{i,j}} \tag{A-1}$$

L_m was the measured power or load and L_c was the corresponding calculated value, index i refers to the actual power/load and index j refers to the wind speed. $w_{1i,j}$ is a weight factor for the actual power/load i at the wind speed j. w_2 is a overall weight factor for the load i.

By minimizing f the calculations will become closer to the measurements and eventually if f becomes zero, the calculations will be identical to the measurements at the wind speeds where measurements and calculations are compared.

The design variables were the airfoil coefficients defined as c_l and c_d as function of α. To limit the number of design variables and to ensure that the results were smooth curves, discrete coordinates determined interpolated curves for c_l and c_d. B-spline curves with k = 5 [8] were used. The c_l and c_d curves were defined for different chord to thickness ratios corresponding to different blade positions. This is equal to the definition of airfoil coefficients in the FLEX4 code and in most other blade element momentum calculations.

An example of the parametric airfoil coefficients is shown in Figure A-1. Six design variables describe c_l and c_d respectively. The design variables have fixed angles of attack but their value of c_l or c_d can be changed and this corresponds to a vertical movement in Figure A-1.

It can in principle not be guaranteed that the resulting c_l and c_d curves are physically obtainable. Possible errors can be non-linear c_l at low angles of attack or misalignment between maximum c_d and rise in c_d due to flow separation. If only few powers/loads are compared to calculations or if the c_l and c_d curves do not contain a proper number of design variables, it is likely that the results will not be realistic. Too few design variables would cause too few degrees of freedom for the airfoil characteristics whereas too many design variables would cause too many possible solutions and most likely oscillations in the airfoil characteristics. Therefore the number of design variables has to be chosen with care with emphasis on the number of available measurements and the reliability of the measurements. Hence no exact definition can be given for the actual design variables used in this work.

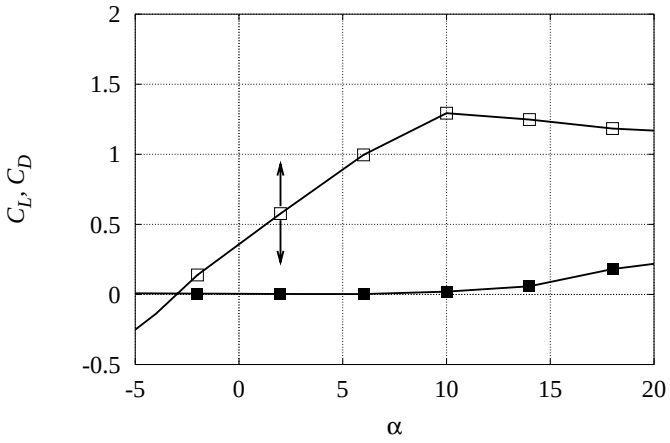

Figure A-1 Parametric curves that describe C_L and C_D versus α. The discrete points are design variables.

A.3 Measurements

The measurements were processed as described in [9] and [10] and the following subset was selected for the analysis:

1. Generator power (and pitch angle)
2. Blade section flapwise moment at rotor radius 2.7 m, $R1_{flap}$.
3. Blade section flapwise moment at rotor radius 6.0 m, $R2_{flap}$.
4. Blade section edgewise moment at rotor radius 2.7 m, $R1_{edge}$.

A FLEX4 model was made of NW46 with LM 21.0ASR to be able to compare the measurements with predictions. Two predictions were made:

- The **initial design** conditions with the theoretically optimum pitch angle. This prediction shows the expected generator power and blade section moments during the design of the LM 21.0ASR blade.
- The **prediction** was made with the measured pitch angle. The measured pitch angle was adjusted during an initial measurement campaign to optimize power. This should correspond to the measurements.

Calibrating the airfoil coefficients for the LM 21.0ASR blade should then eliminate the discrepancy between the **prediction** and the measurement, whereas the performance of NW46 with LM 21.0ASR should be compared with the **initial design**.

A.3.1 Corrections

The calibration of the $R1_{flap}$, $R2_{flap}$ and $R1_{edge}$ strain gauge measurements on the blades was done using the blade weight, which is a method that is associated with some uncertainty. The predictions at low wind speeds should be in good agreement with measurements because the airfoil coefficients at low angles of attack are very reliable. Comparing predictions at low wind speeds with the measurements was therefore used to evaluate the calibration. This resulted in off-set corrections for the measurements as shown in Table A-1.

Table A-1 Offset correction of measurements to match the predictions.

Load	Offset
$R1_{flap}$ (kNm)	-48.8
$R2_{flap}$ (kNm)	-52.7
$R1_{edge}$ (kNm)	-66

No calibrations were done for power and pitch angle.

A.3.2 Average results versus wind speed

Figure A-2 and Figure A-3 show generator power and generator CP respectively. It can be seen that the agreement between the **measurements** and the **initial design** prediction is good at low wind speed and that CP is somewhat better in the **measurement** compared with the **initial design** prediction. At the 'knee' of the power curve and at high wind speeds the **measurement** shows a lower power compared with the **prediction** on basis of the actual pitch angle. This difference is due to the influence of turbulence and the difficulties for the pitch regulation system to maintain the optimum pitch angle. At high wind speeds above 11 m/s the difference between the **measurement** and the **prediction** is due to the discrepancy between the initial airfoil coefficients and the actual airfoil coefficients.

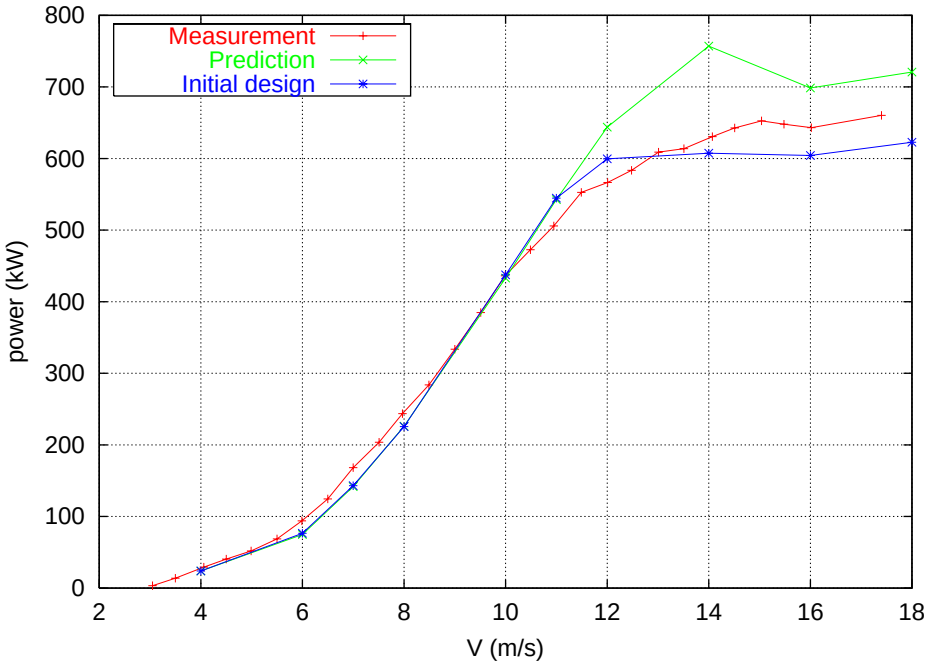

Figure A-2 Generator power versus wind speed.

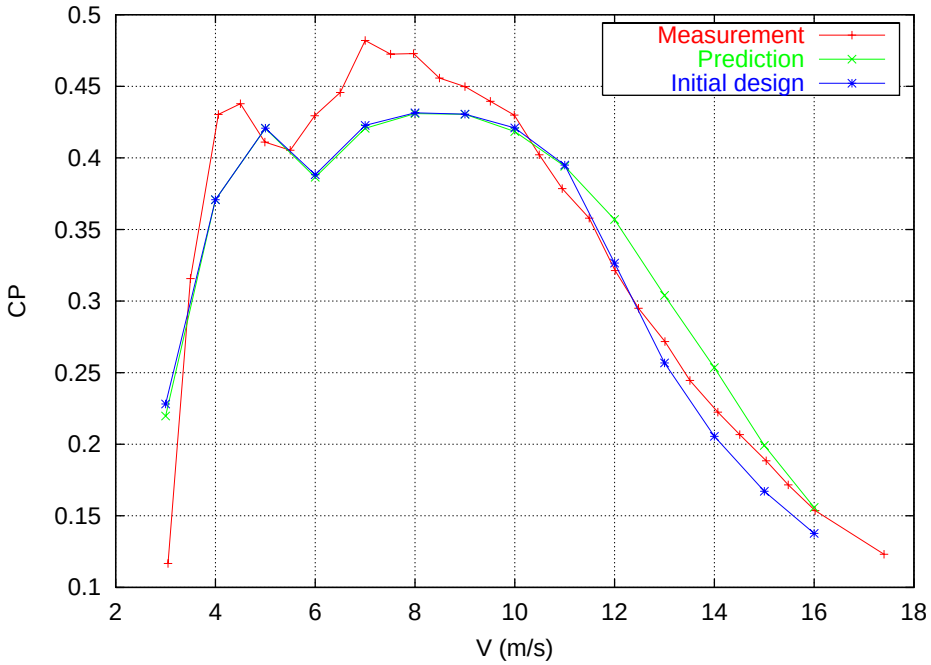

Figure A-3 CP versus wind speed.

Figure A-4 shows the **measured** pitch angle compared with the **initial design** pitch angle. A significant difference can be seen both at low and high wind speed, which indicates a discrepancy between the actual airfoil coefficients and the initial design airfoil coefficients. The difference at low wind speed is not significant and it has only little influence on power. However, the difference at high wind speeds indicates that the stall of the blade is different compared to the expected behavior during the **initial design**.

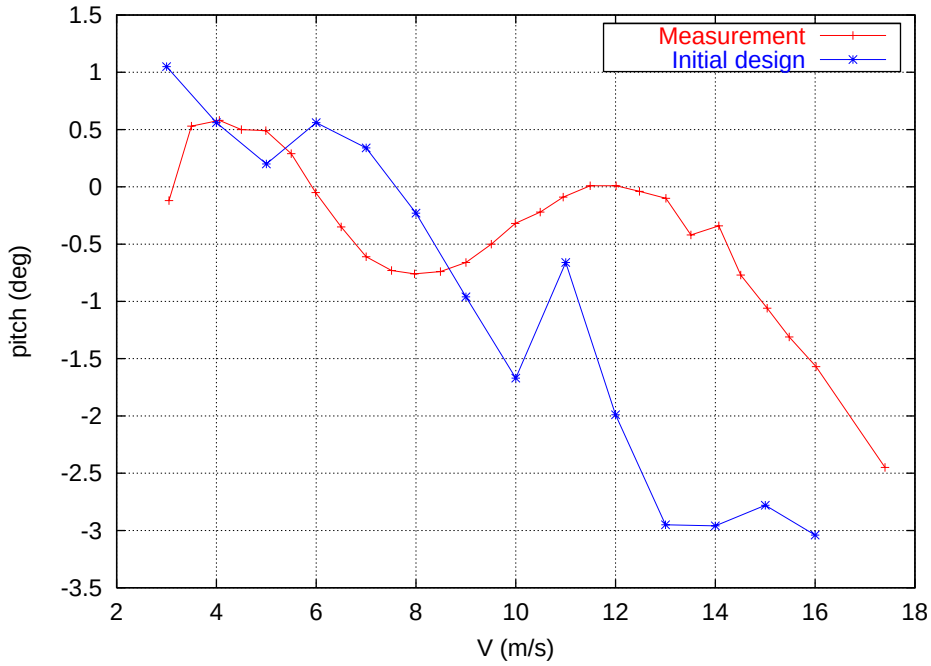

Figure A-4 Pitch angle versus wind speed.

Figure A-5, Figure A-6 and Figure A-7 show measured section moments compared to predictions. The **measurements** were offset to match the predictions at low wind speeds as explained in Section A.3.1. For $R1_{flap}$ (Figure A-5) very good agreement is seen at wind speeds below 10 m/s between the **measurement**

and the **prediction** with the actual pitch angles. At wind speeds above 10 m/s the measured load is below the predictions.

For $R2_{flap}$ (Figure A-6) the trend is similar to $R1_{flap}$ but the agreement is not as good at low wind speeds. This may be either due to the calibration of the measurement or due to uncertainty on the exact location and orientation of the strain gauges.

The $R1_{edge}$ measurement (Figure A-7) is scattered, which makes the comparison with the predictions difficult. The slope of the **measurement** is in fair agreement with the predictions between 8 m/s and 12 m/s.

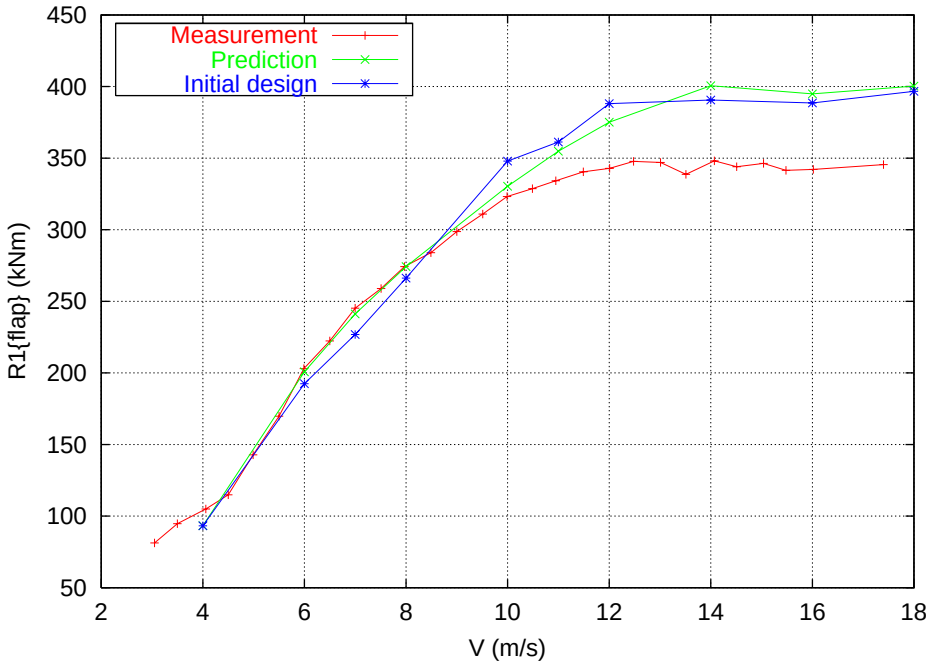

Figure A-5 $R1_{flap}$ versus wind speed.

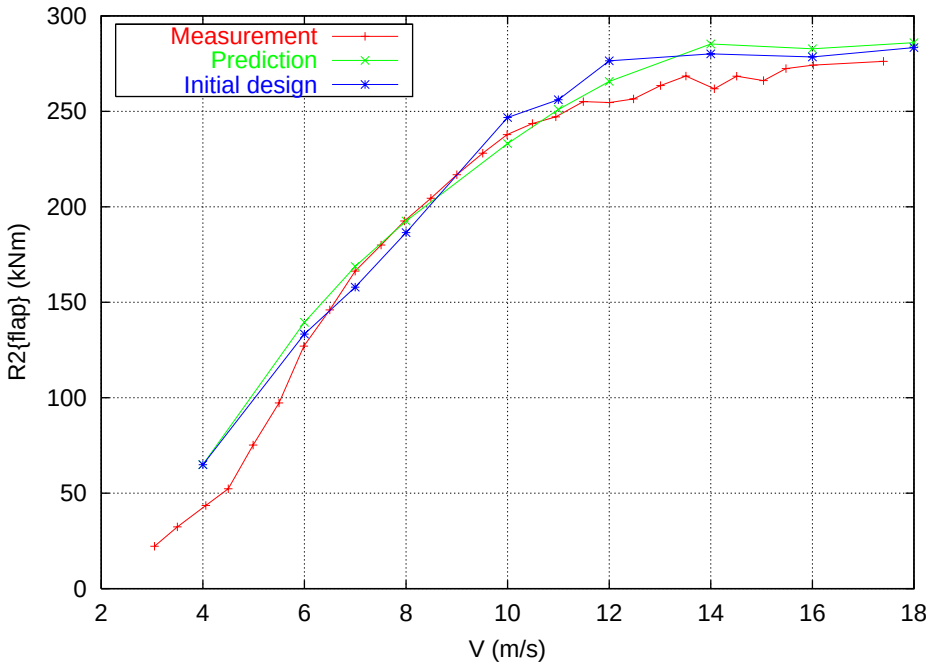

Figure A-6 $R2_{flap}$ versus wind speed.

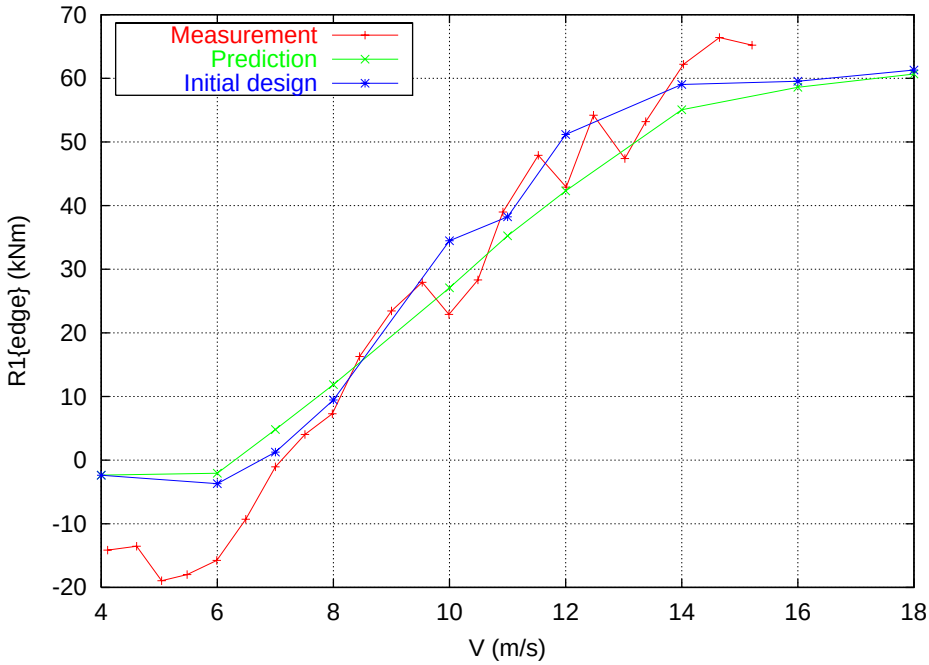

Figure A-7 $R1_{edge}$ versus wind speed.

A.3.3 Measurement selection

The good agreement between the measurements and the predictions at low wind speeds for the generator power and $R1_{flap}$ verified the calibration of these load sensors. Therefore they were selected for the inverse determination of the airfoil coefficients.

The validity of $R2_{flap}$ and $R1_{edge}$ was more questionable because of scatter ($R1_{edge}$) and uncertainty of the calibration of the strain gauges ($R2_{flap}$).

In summary we decided to use the generator power and $R1_{flap}$ to calibrate the airfoil coefficients and then use $R2_{flap}$ and $R1_{edge}$ only in the evaluation of the derived airfoil coefficients.

A.4 Results

The selection of measurements with generator power and only one blade section moment must be categorized as an absolute minimum to be able to derive airfoil characteristics. Having more section moments would have allowed for a more ambitious derivation and for better accuracy of the derived results.

It was found realizable to select two airfoil sections for the inverse determination of airfoil coefficients as shown in Table A-2. The Risø-A1-15 section represents the blade tip whereas the Risø-A1 (18% to 24%) represents the outer part of the blade as a single average of the airfoil coefficients. A more detailed division of the blade would have required more section moments available.

All together the selected airfoil characteristics cover the part of the LM 21.0ASR blade without vortex generators from 12 m until 23 m.

Table A-2 Selected airfoil sections for inverse determination of airfoil coefficients.

Airfoil section	Thickness	Radial position
Risø-A1-15	15%	23 m (blade tip)
Risø-A1 (18% to 24%)	18% to 24%	12 m until 20 m

The design variables for the airfoil sections were c_l and c_d in the angle of attack range from 6^o until 25^o. Both c_l and c_d was represented by a B-spline defined from between four to six control points.

The optimisation objective was the RMS between the calculated generator power and $R1_{flap}$ (predicted by FLEX4) and the measurements. Measurements from 8, 9, 10, 11, 12, 13, 14 and 15 were used with equal weight.

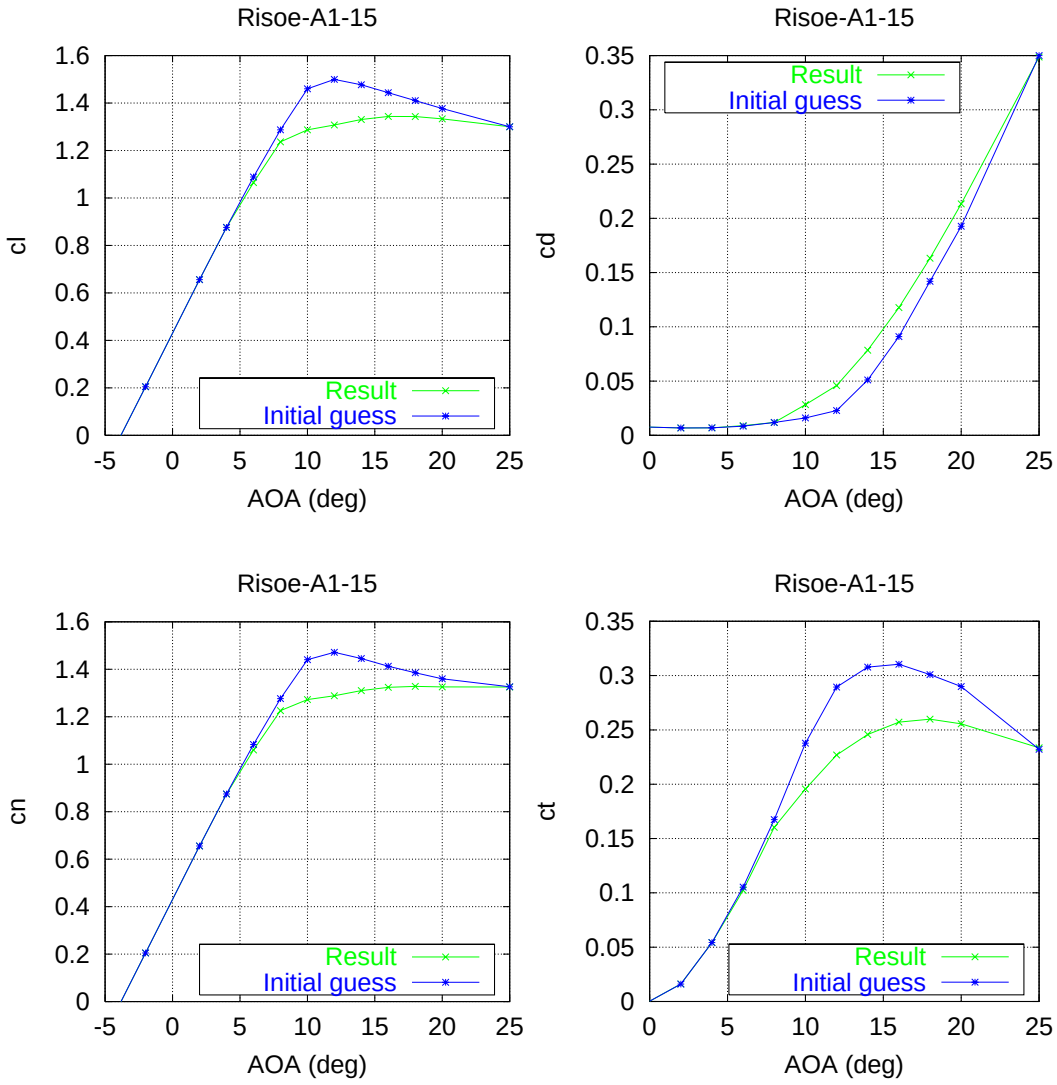

Figure A-8 Airfoil characteristics for Risø-A1-15.

A.4.1 Airfoil characteristics

Figure A-8 and Figure A-9 shows the **resulting** derived airfoil coefficients for Risø-A1-15 and Risø-A1 (18% to 24%) respectively compared with the **initial guess**, which was used for the initial design prediction. For reference, Figure A-10 shows the airfoil characteristics for the inboard part of the LM 21.0ASR blade with vortex generators. In addition to c_l and c_d, the driving force component, c_t, is shown together with the normal force component, c_n.

The Risø-A1-15 **resulting** airfoil at the blade tip (Figure A-8) shows a reduced maximum c_l and an earlier drag rise compared to the **initial guess**. This trend is in agreement with the general trends identified in [2]. With the general knowledge of 3D airfoil coefficients for the tip, this discrepancy is not surprising but should have been foreseen during the initial design. The slope of c_l at angles of attack between 0 and 6 degrees is in good agreement between the **resulting** airfoil coefficients and the **initial guess**.

The Risø-A1 (18% to 24%) **resulting** airfoil coefficients (Figure A-9) shows a drop in maximum c_l compared with the **initial guess** on 1.42 to 1.19. The slope of c_l versus angle of attack is maintained until 6^o. The drop in maximum c_l indicates an earlier stall of the airfoil than what was expected from the 2D wind tunnel measurements [11]. Also the result for c_d during stall is different than the initial guess with a lower drag from 11 to 20 degrees. The different c_l and c_d result in a significant reduction of c_t from 8 until 18 degrees, which is the cause of the discrepancy between the actual measured power and the prediction in Figure A-2. The difference in c_n explains why the measured $R1_{flap}$ is lower than prediction in Figure A-5.

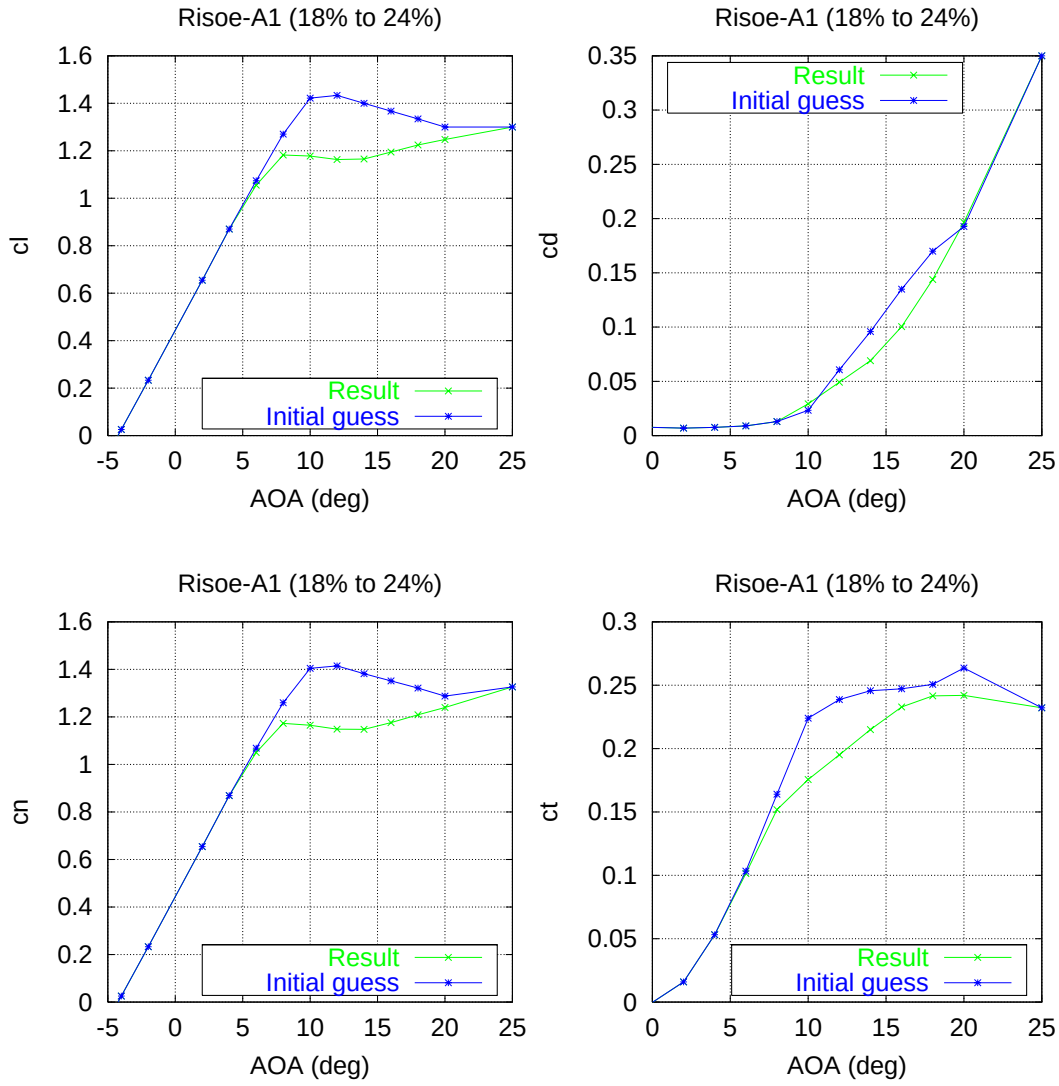

Figure A-9 Airfoil characteristics for Risø-A1 (18% to 24%).

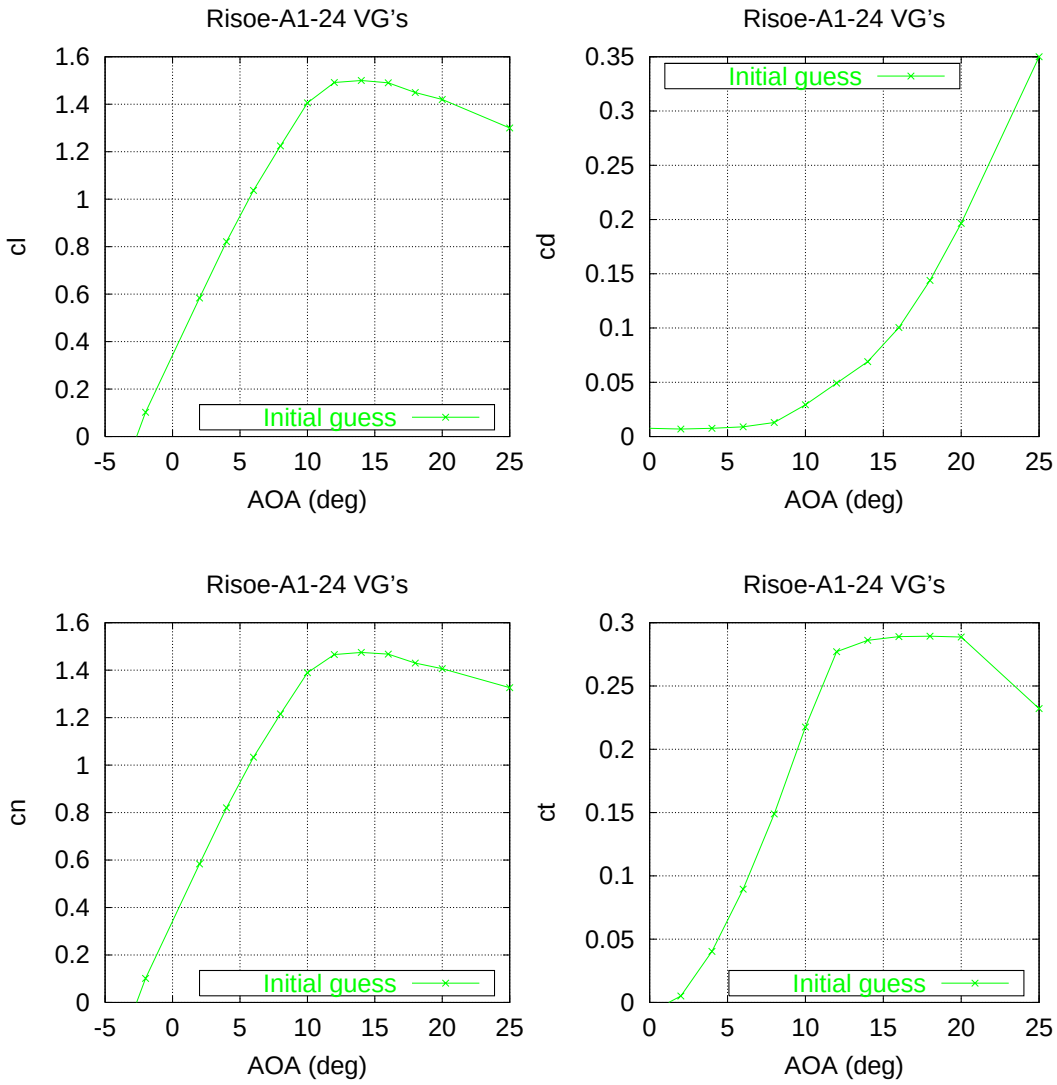

Figure A-10 Airfoil characteristics for Risø-A-24 with vortex generators used for the inboard part of the Lm 21.0ASR blade.

A.4.2 RMS Error

Figure A-11 shows the RMS of the involved sensors for the initial guess of the airfoil coefficients compared with the result. It can be seen that the RMS was reduced for both sensors at all the involved wind speeds with small differences corresponding to the scatter in the measurements. A significant reduction in the RMS can be seen as a result of the justification of the airfoil coefficients, which indicates a better match between measurements and predictions.

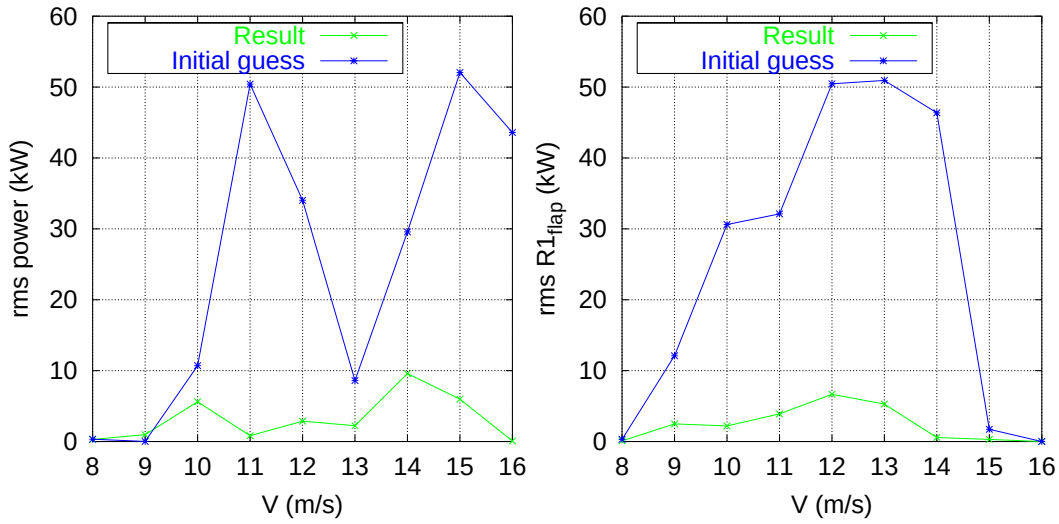

Figure A-11 RMS for generator power and $R1_{flap}$ versus wind speed.

A.5 Evaluation of results

This chapter shows the comparison of the resulting performance with the derived airfoil data with the measurements. To evaluate the results, the derived airfoil characteristics were compared with the available 2D wind tunnel measurements from the VELUX wind tunnel and the actual aerodynamic operation of the NW46 with the LM 21.0ASR blades was detected.

A.5.1 Measurements and predictions

Figure A-12 shows the comparison of the **measured** generator power with the **uncorrected prediction** on basis of the initial guess on the airfoil data and the **corrected prediction**, which resulted from the justification of the airfoil coefficients. It can be seen that very good agreement appeared at high wind speeds between the **measurement** and the **corrected prediction**.

Figure A-13, Figure A-14 and Figure A-15 show comparisons of the **measured** blade section moments and the **uncorrected** and corrected predictions.

The agreement between the **measured** $R1_{flap}$ and the **corrected prediction** (Figure A-13) improved significantly compared with the **uncorrected prediction**. However, the trend at high wind speeds is still somewhat different for the **corrected prediction** compared with the **measurement**. It was not possible to find a combination of airfoil data to match better $R1_{flap}$ and at the same time to match the generator power.

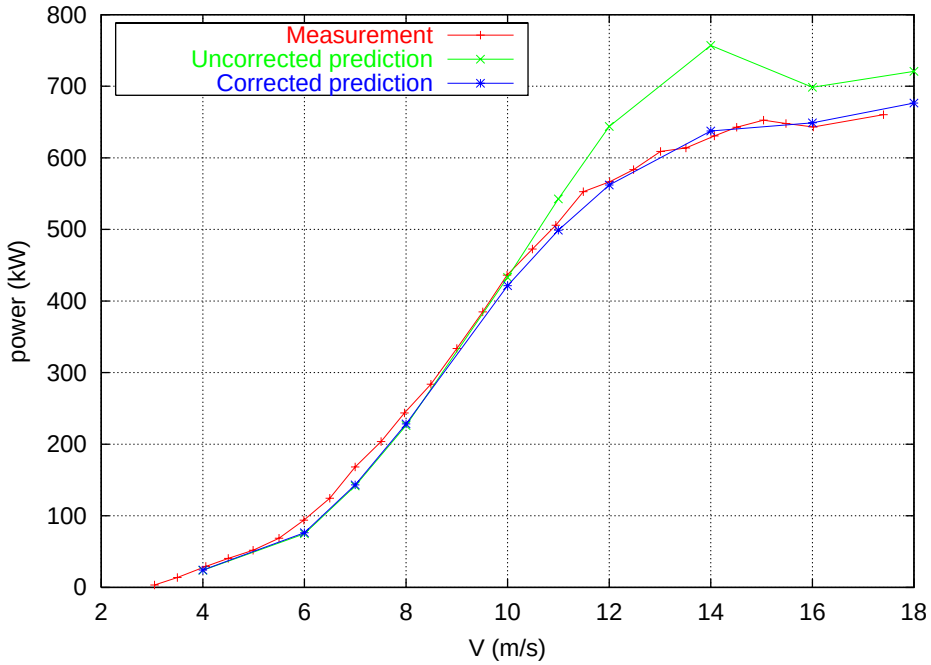

Figure A-12Generator power versus wind speed.

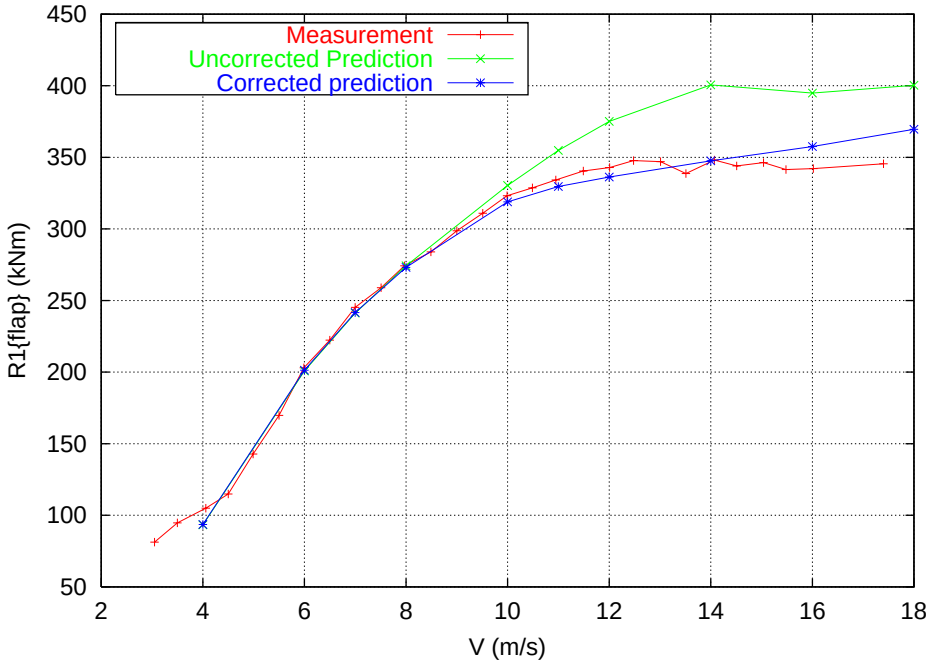

Figure A-13 $R1_{flap}$ versus wind speed.

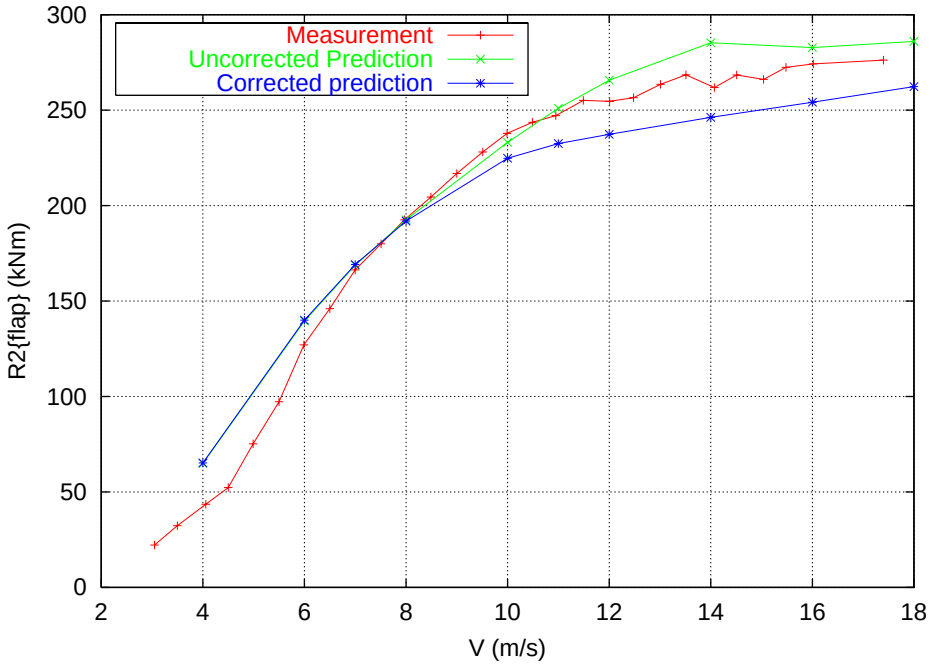

Figure A-14 $R2_{flap}$ versus wind speed.

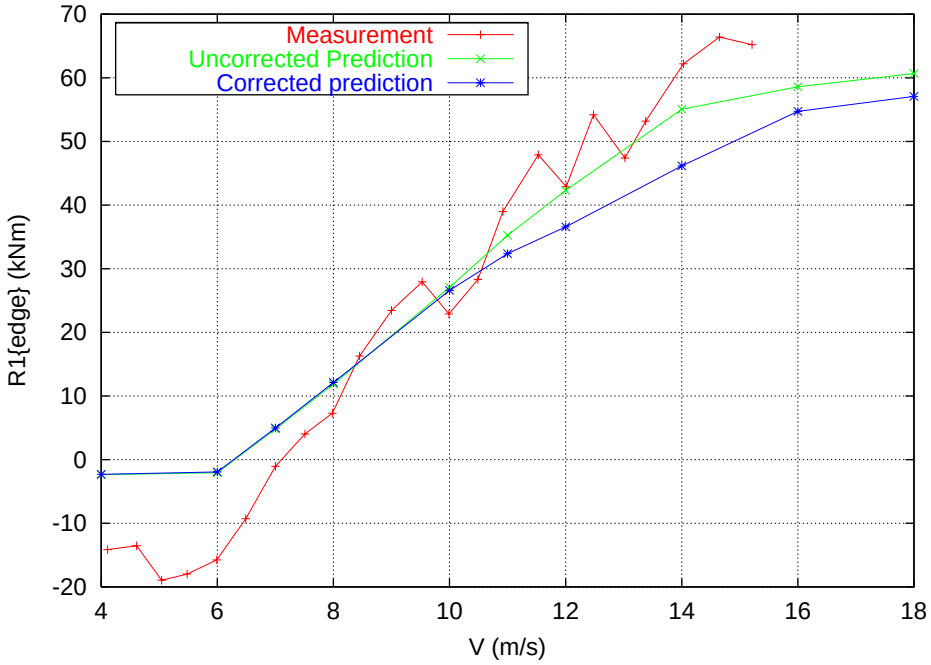

Figure A-15 $R1_{edge}$ versus wind speed.

A.5.2 Airfoil characteristics

The resulting airfoil characteristics were compared with the available 2D wind tunnel measurements from [11].

Figure A-16 shows the **results** for Risø-A1-15 compared with 2D VELUX wind tunnel measurements of Risø-A1-18 with **smooth surface** and with leading edge roughness (**LER**) respectively. 2D Measurements were not available for Risø-A1-15. The **results** at angles of attack above 15 degrees were different due to the three-dimensional flow of the rotor and it is well known that 2D measurements cannot be trusted in this region [2]. The slope of the **resulting** c_l before maximum c_l was in very good agreement

with the VELUX measurement with **smooth surface**. The value of maximum cl and the rise in cd from separation felt in between the **smooth** and the **LER** measurements with a better match to the **smooth** measurement compared with the **LER** measurement. This indicated that the cause of the difference between the result and the initial guess is the 3D rotational effects rather than surface roughness.

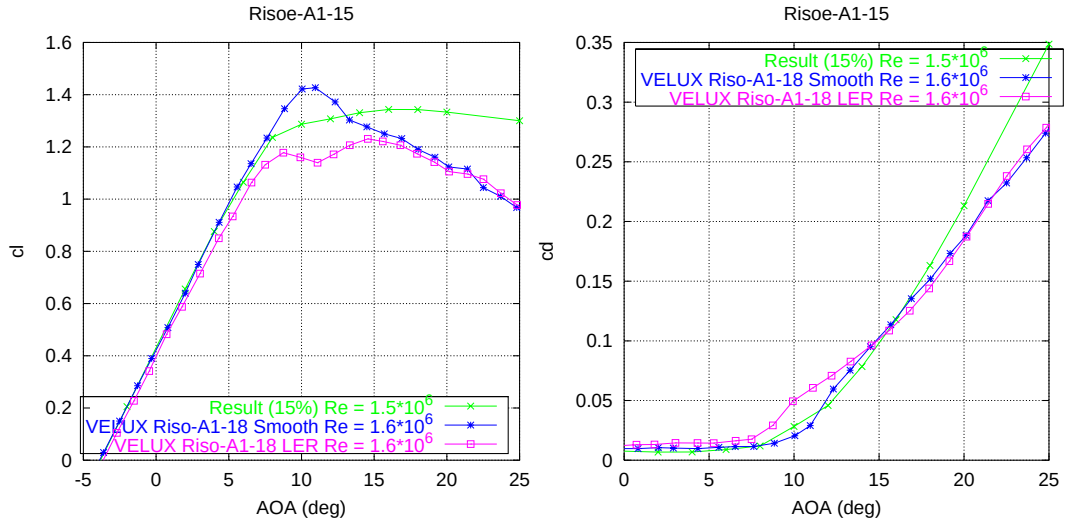

Figure A-16 Airfoil characteristics for Risø-A1-15 on LM 21.0ASR compared with 2D VELUX measurements of Risø-A1-18 for smooth flow (Smooth) and with leading edge roughness (LER).

Figure A-17 and Figure A-18 show the **resulting** airfoil characteristics for Risø-A1 (18% to 24%) compared with 2D VELUX measurements of Risø-A1-18 (Figure A-17) and Risø-A1-24 (Figure A-18). There was a very good agreement between the **resulting** maximum c_l and the maximum c_l for both Risø-A1-18 and Risø-A1-24 with **LER**. This indicates that proper airfoil characteristics for this part of the blade should be based on measurements with a rough surface. This may be because the airfoils in themselves are sensitive to roughness or imperfections on the leading edge shape but also because of the high relative thickness, which may cause a different 3D flow compared to the 2D measurements.

It can be concluded that the discrepancy between the measured generator power and the initial design prediction is mainly due to the lack of proper airfoil characteristics for Risø-A1 (18% to 24%) and that this can be accounted for by using airfoil data with leading edge roughness for this part of the blade.

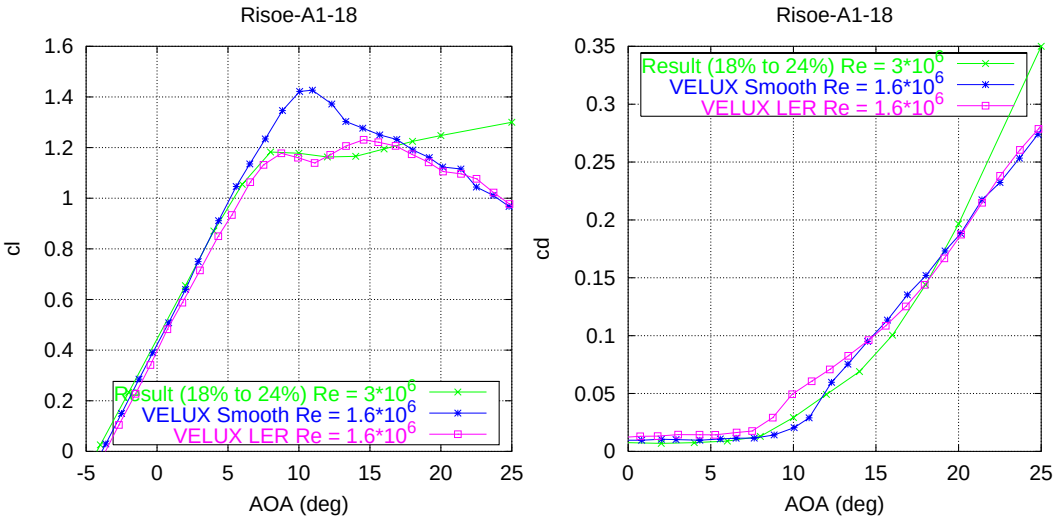

Figure A-17 Airfoil characteristics for Risø-A1 (18% to 24%) on LM 21.0ASR compared with 2D VELUX measurements of Risø-A1-18 for smooth flow (Smooth) and with leading edge roughness (LER).

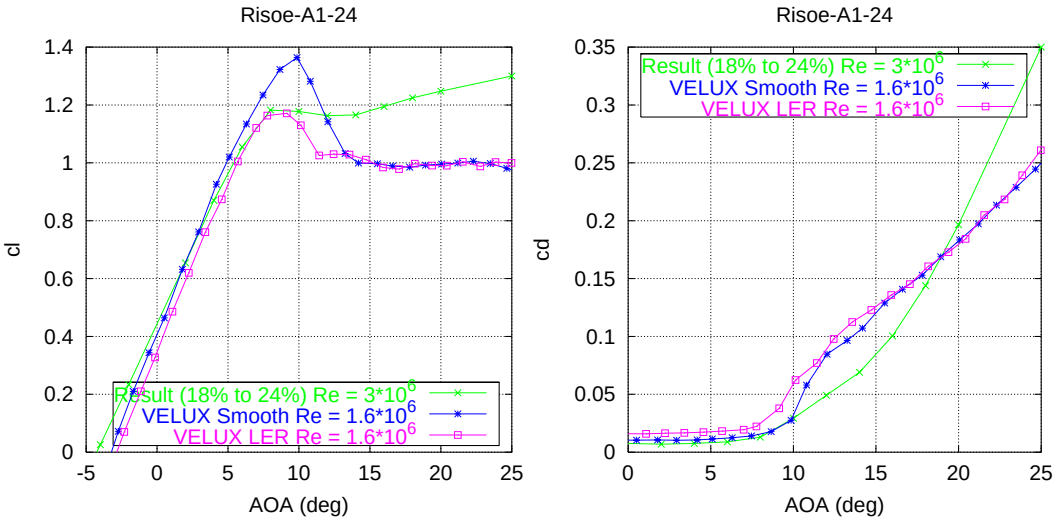

Figure A-18 Airfoil characteristics for Risø-A1 (18% to 24%) on LM 21.0ASR compared with 2D VELUX measurements of Risø-A1-24 for smooth flow (Smooth) and with leading edge roughness (LER).

A.5.3 Analysis of operation of NW 46

The operation of NW46 with LM 21.0 ASR blades can be seen in Figure A-19 and Figure A-20 for the Risø-A1-15 airfoil at the blade tip (Figure A-19) and for the Risø-A1 (18% to 24%) (Figure A-20). It can be seen for both airfoil sections that the LM 21.0ASR blade operated around maximum c_l on the outer part of the blade and that the areas covered are from 4 to 11 degrees for Risø-A1-15 and from 6 to 15 respectively 18 for the Risø-A1-18 and Risø-A1-24.

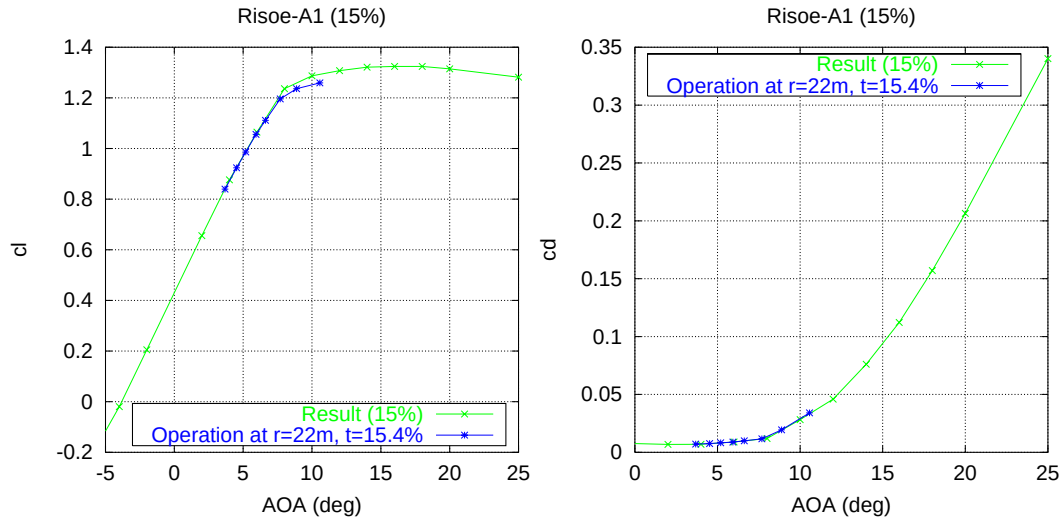

Figure A-19 Risø-A1-15% operation points for cl and cd at r=22m, t=15.4% from v=8m/s to 15m/s.

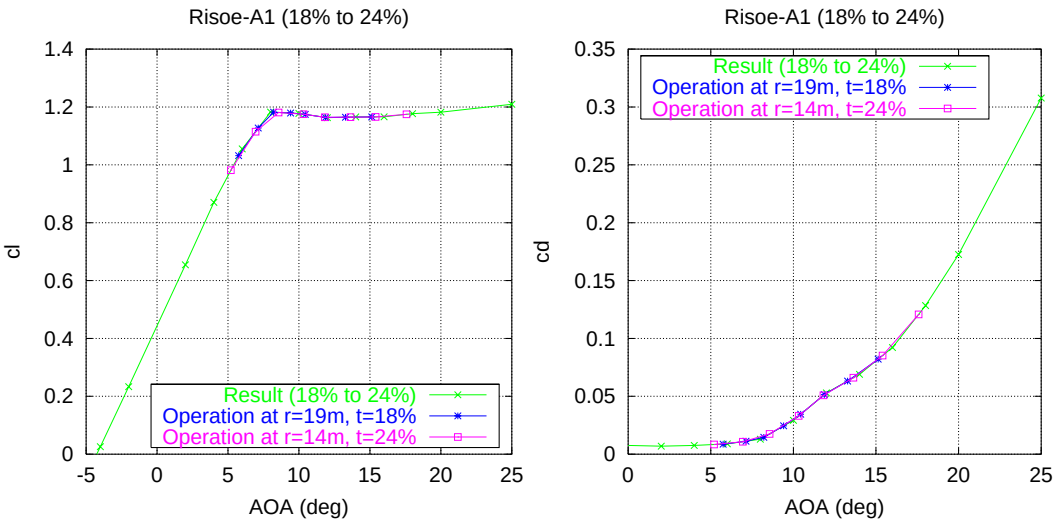

Figure A-20 Risø-A1 (18% to 24%) operation points for cl and cd at r=14m, t=24.0% and r=19m, t=18% from v=8m/s to 15m/s.

B Power-curve and load assessment of LM 21.0 ASR blades

B.1 Introduction

To evaluate the new blade design it was necessary to carry out a comprehensive measuring program. The focus for the program was to measure the power curve and the blade loads, because this would make it possible to determine the overall performance of the blade in term of energy output to load ratio compared to the traditional blade.

Since at the same time marginal improvements were expected, at least with respect to the power performance, it was deemed necessary to make simultaneous measurement on a traditional blade on a nearly identical turbine. A measuring setup was therefore chosen where simultaneous measurements were carried out on two NORWIN 46-ASR-600 kW turbines placed approximately 5 rotor diameters apart and with a wind speed and direction measuring mast in between and slightly south of the turbines.

If the success criteria's for the new blade design should be met the result of the measurements should be an improved energy output to load ratio compared to the traditional blade. However, it would be desired that the energy output did not decrease compared to the traditional blade even though the loads decreased further, since a competitive turbine using the new blade design would then need to have a larger rotor diameter to compensate. This would will make the results much more difficult to evaluate.

The measurements took place over a period of one and a half year, starting with fine tuning of operational parameters, then power curve measurements and finally a combination of power curve measurement and load measurements.

The power performance evaluation process was to compare the measured power curves for the two turbines for the whole measuring period, resulting in a final measure for the difference in energy output between the turbines.

The load evaluation process was slightly more complicated, because the measured quantities and statistical derivatives is not the result of most significance. Seen in perspective of the turbine running in the normal operating range, the most important figures to evaluate are the fatigue loads, and since calculation of fatigue loads is quite time consuming, it was decided not to work on the complete measured series, but to limit the analysis to a representative measuring series.

Based on the representative measuring series the strategy for the loading analysis and the evaluation of the blade design was to follow a two-step process. First, to prove that the measured loads and the loads calculated with an aeroelastic model, using the in chapter A deriver airfoil coefficients and the measured turbulence and air density, gave equal results. Secondly, to use aeroelastic calculations to compare energy output and loads between the new design blade and the traditional blade.

It should be mentioned that going through the aeroelastic model for comparison is only the second best way. However, since blade measurements were not made on the traditional blades, the loads could not be compared directly. This gives the analysis results a slightly higher uncertainty.

B.2 Measuring setup

B.2.1 Equipment

Figure B-1 The Norwin 46-ASR-600 kW turbines Ørsted 2 (in front) and Ørsted 1 used in the measuring program. The wagon containing the measuring equipment is seen besides Ørsted 2, and the measuring mast is seen to the left of the road.

The main equipment used in the measuring program was (see also Figure B-1):

- Norwin 46-ASR-600 kW wind turbine Ørsted 2, equipped with traditional LM 21.0 P blades.
- Norwin 46-ASR-600 kW wind turbine Ørsted 1, equipped with the new design LM 21.0 ASR blades.
- Measuring mast with Risø Anemometer, and vind vane.
- Surroundings temperature and pressure measured on top of the Ørsted 2 turbine.
- Power measurement equipment on both the Ørsted 1 and Ørsted 2 turbine.
- Stain gauge load measurements on the Ørsted 1 turbine in the root section of the LM 21.0 ASR blade (0.7 m from the blade root flange) flapwise and edgewise and flapwise in 2 sections: 4 meters and 6 meters from the blade root flange. The strain gauge signals were amplified and transmitted to the fixed system via electrical slip rings.
- Measuring computer equipped with a National Instruments measuring card, Labview measuring software and various amplifier and connector modules.

The normal sample rate for the measurements was 40 Hz.

The power curve measurements took place for a period of approximately a year, with the results successively evaluated. During the campaign a number of down periods were encountered, mainly because the cables to the measuring mast was cut in pieces by farming machinery. In one incident the damages resulting from a lightning strike meant that a large part of the equipment had to be replaced.

During the blade comparison measurement period the turbine were running with the most simple type of blade regulation, where the blade angle pitch setting was defined according to a fixed table linking wind speed and pitch angle. The reason for this choice was first that it would make the analysis of the measuring results much easier, than if the turbine would regulate itself according to a complex procedure. Second, that the results could be publicized without restrictions because Norwin do not consider the simple regulation method as critical knowledge. A number of tests and adjustments to optimize the regulation were conducted before commencing the actual power curve measurements.

The load measurements took place for a period of approximately 5 months. Unfortunately it was clear from the beginning that the strain gauges placed in station 3 from the blade root was damaged either during transport or erection of the blade and it was not possible to get to this position afterwards. The rest of the strain gauges were apparently functioning, but when the final analysis was made it turned out that apart from the measured power only the flapwise blade bending in radius 0.7 m from the blade root flange could be fully trusted all through the period. Luckily it was enough to be able to draw a conclusion.

During the period, LM Glasfiber initiated a noise measurement carried out by Ingemansson Technology A/S. This showed that the noise level from Ørsted 1 with LM 21.0 ASR blades was: 98.8 dBA.

The LM 21.0 ASR blades are equipped with vortex generators, and since they did not behave exactly as theoretically supposed, the idea came up that the part of the blade equipped with Vortex generators was maybe to long. To test this assumption a part of the Vortex generators were taken off, and at the very end of the project a short measuring campaign was made to study the result. The results of these tests are not addressed in this report.

B.3 Power curve assessment

In Figure B-2 to Figure B-7 the main results from the power curve measurements are plotted. The points in the plots, except for the binned values, represent a value derived from a measured series of 10 minutes duration.

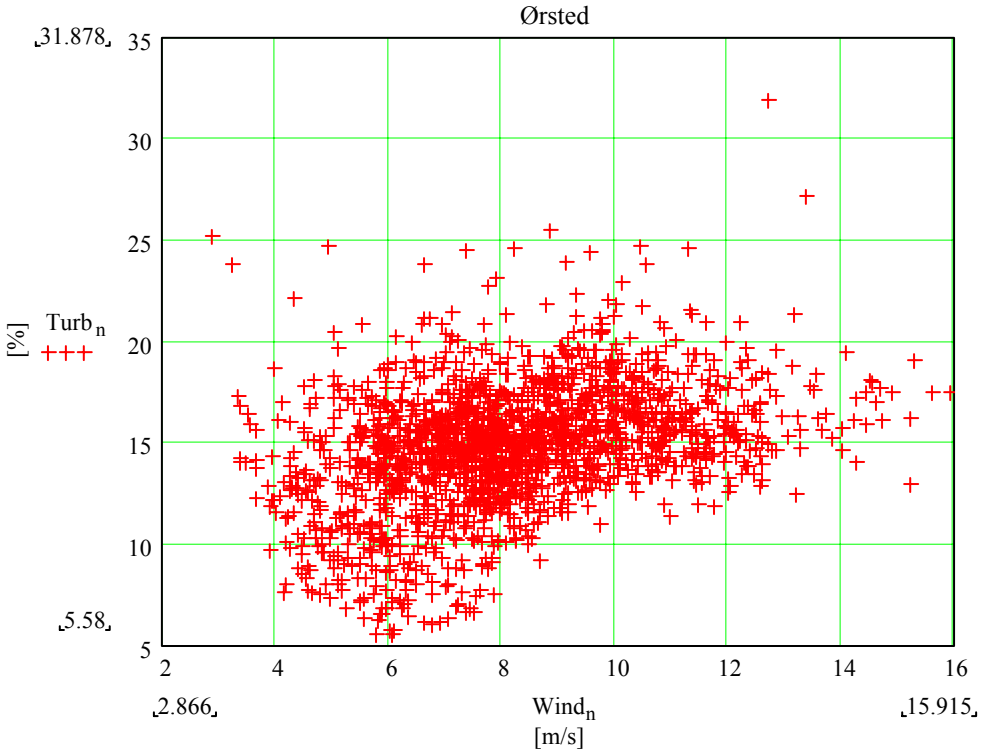

Figure B-2 Power curve for Norwin 46 turbine with LM 21.0 P blades shown as 10 minutes average points, maximum and minimum peak value within the 10 minutes, and standard deviation.

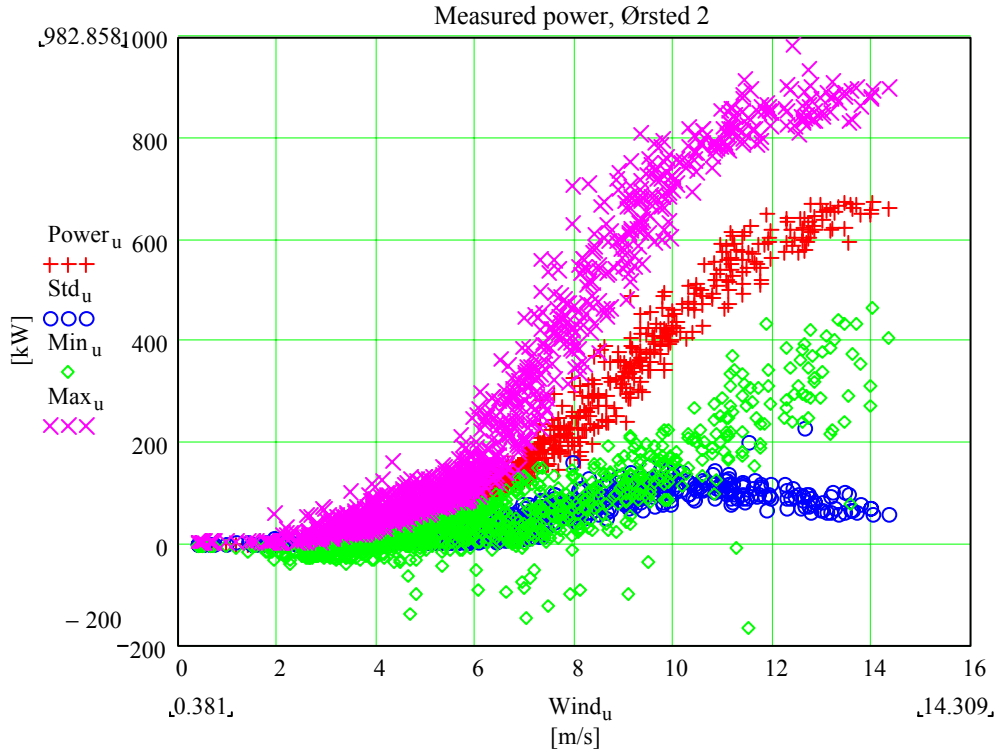

Figure B-3 Power curve for Norwin 46 turbine with LM 21.0 P blades shown as 10 minutes average points, maximum and minimum peak value within the 10 minutes, and standard deviation.

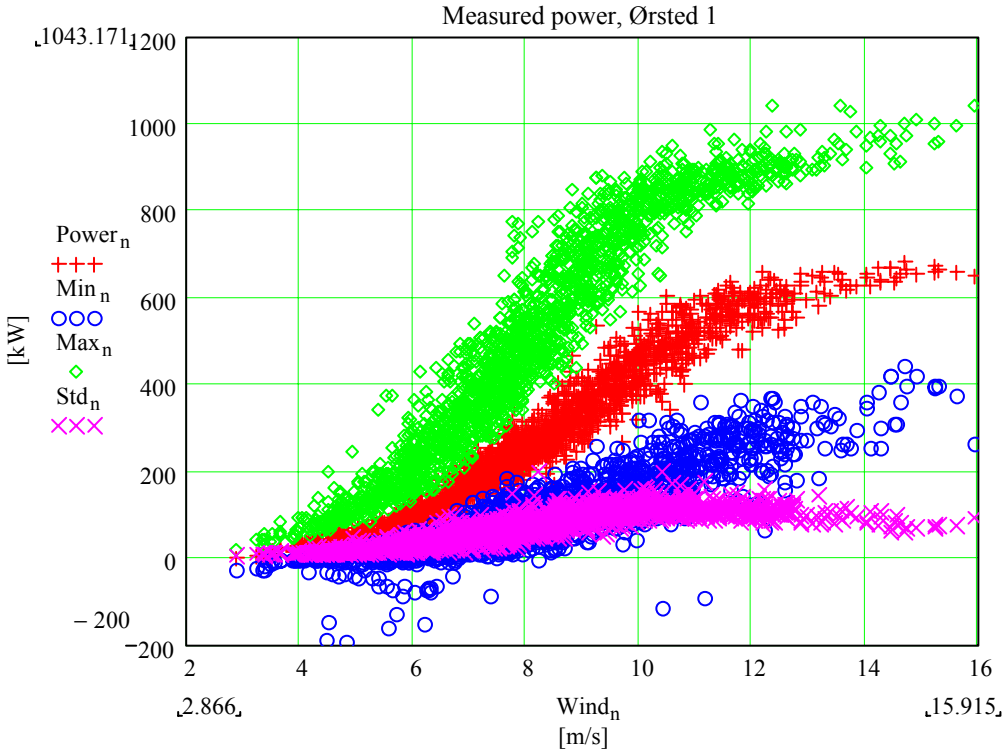

Figure B-4 Power curve for Norwin 46 turbine with LM 21.0 ASR blades shown as 10 minutes average points, maximum and minimum peak value within the 10 minutes, and standard deviation.

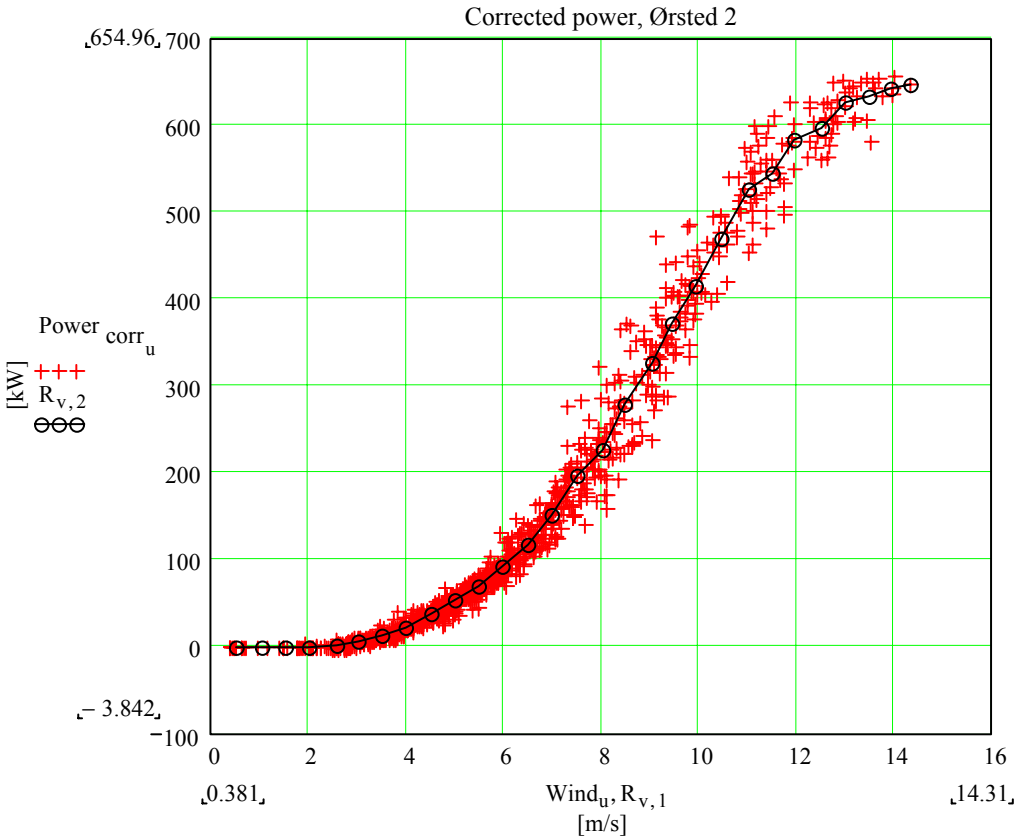

Figure B-5 Power curve for Norwin 46 turbine with LM 21.0 P blades shown as 10 minutes average points and binned values, corrected to air density 1.225 kg/m^3.

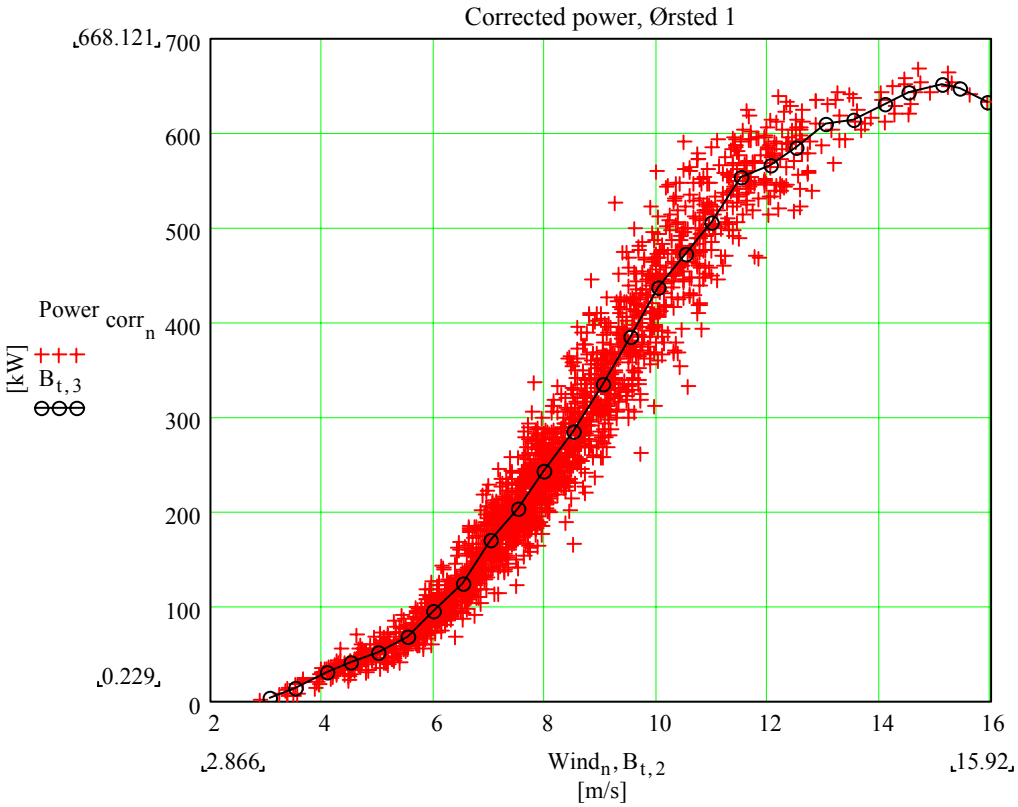

Figure B-6 Power curve for Norwin 46 turbine with LM 21.0 ASR blades shown as 10 minutes average points and binned values, corrected to air density 1.225 kg/m^3.

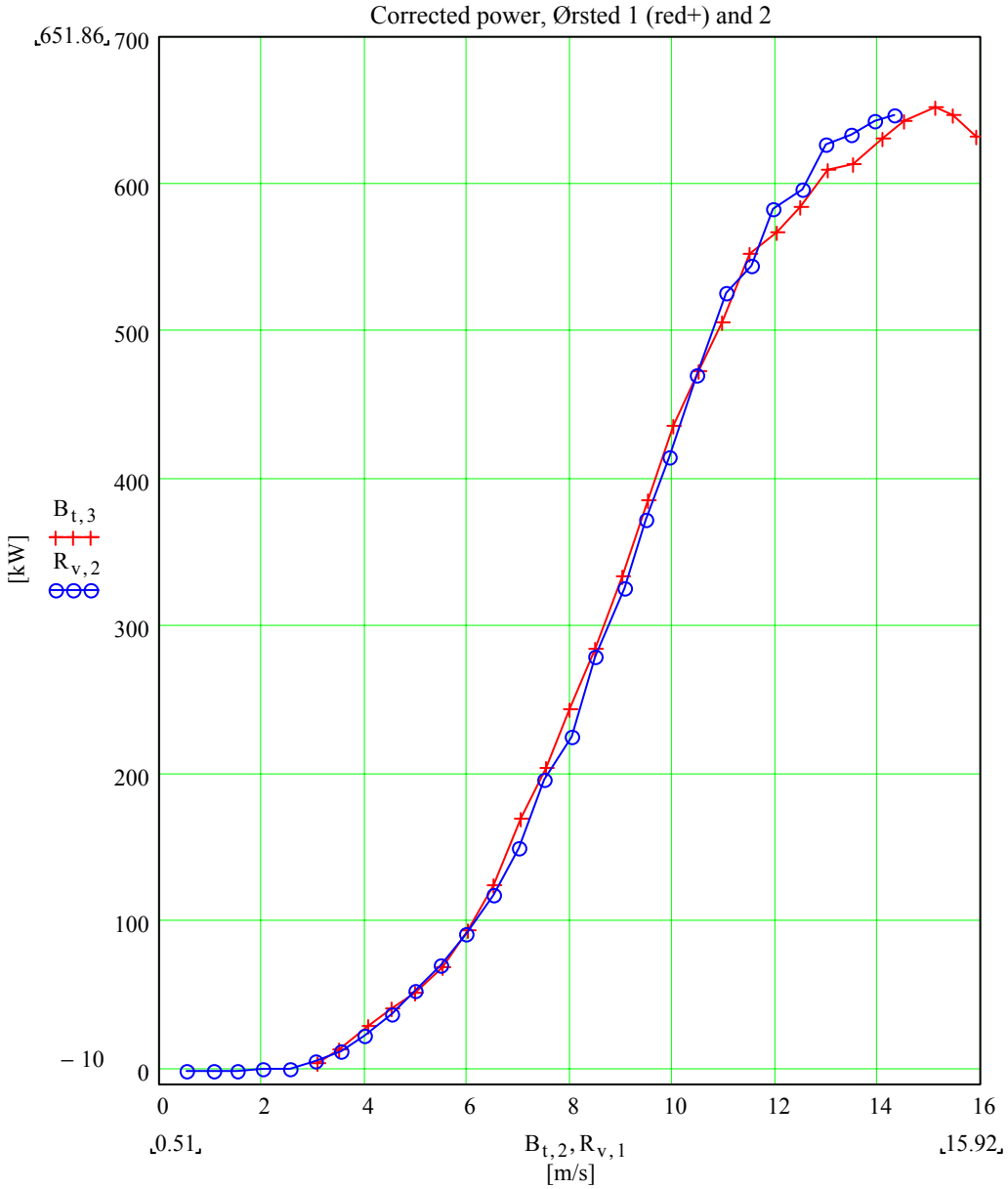

Figure B-7 Power curve for Norwin 46 turbine with LM 21.0 ASR blades compared with LM 21.0 ASR blades shown as binned values, corrected to air density 1.225 kg/m^3.

In Figure B-2 it is seen that the turbulence on the site is relatively high even at high wind speed, which makes it suited for testing a blade where the control properties of the design is important. If a site with low turbulence were chosen, then the negative effects of a blade with poor properties for controllability would have been difficult to reveal.

Figure B-3 and Figure B-4 shows the measured power for the Ørsted 2 N46 turbine with traditional LM 21.0 P blades and the Ørsted 1 N46 turbine with the new LM 21.0 ASR blades. In both cases maximum, average value, minimum and standard deviation is plotted.

Two things should be noticed. First, some of the minimum values are observed to be far below 0 kW, which means that the turbine is executing a stopping sequence or a shift between the two generators during the measuring period. Second, the shapes of the point clouds for the two turbines are different around 6 m/s to 7 m/s. It was unfortunately not discovered before afterwards that the parameters for shifting between the two generators were set differently, resulting in a slightly poorer power curve for the Ørsted 2 turbine in the wind speed range from approximately 7 m/s to 9 m/s.

Figure B-5 and Figure B-6 shows, for the two turbines, the point cloud of average values for the electrical power corrected to standard air density 1.225 kg/m3, together with the binned value of the same.

In Figure B-7 the power curves for the two turbines are plotted together, and in Table B-1 the specific figures are shown.

It is found that the figures are fairly similar, with a tendency that the power curve from the turbine with the new LM 21.0 ASR has a slightly better performance, except in the wind speed range from 12 m/s to 14 m/s (explained in A). This is in correspondence with the operational experience from the turbine, where it is found that the energy output from the two turbines is almost the same.

Table B-1 Power curves for Norwin 46 with LM 21.0 P and LM 21.0 ASR corrected to air density 1.225 kg/m^3. Description of columns:

Ørsted 2 - N46 - LM 21.0 P				**Ørsted 1 - N46 - LM 21.0 ASR**			
Wind speed [m/s]	Corrected power [kW]	Power std.dev. [kW]	Number	Wind speed [m/s]	Corrected power [kW]	Power std.dev. [kW]	Number
3.03	5.31	3.26	60	3.05	3.37	4.44	2
3.51	12.21	4.42	78	3.50	13.78	7.00	11
3.98	22.22	6.94	87	4.06	29.32	6.92	19
4.50	37.34	6.48	92	4.50	40.61	9.55	48
4.99	53.29	9.72	96	4.99	51.99	9.79	58
5.47	69.52	9.96	107	5.50	68.64	12.57	79
5.96	91.28	15.26	80	5.99	94.08	15.95	143
6.49	117.96	17.24	53	6.51	124.74	22.86	123
6.98	150.08	20.77	50	7.01	168.86	28.29	154
7.48	195.92	32.47	43	7.51	204.10	30.14	223
8.00	225.12	36.62	35	7.97	243.72	30.90	192
8.47	279.15	48.91	28	8.49	284.25	43.20	143
9.03	325.66	47.08	31	9.00	334.05	43.49	132
9.45	371.54	39.38	30	9.51	384.84	47.15	117
9.91	414.85	37.39	24	9.99	436.30	47.57	85
10.44	469.90	33.82	14	10.49	472.62	53.29	84
11.01	525.55	39.24	25	10.95	505.88	40.19	60
11.51	544.01	35.38	18	11.49	552.67	33.77	57
11.94	582.78	25.88	7	12.01	566.60	33.03	39
12.52	596.50	21.86	17	12.48	583.56	29.90	32
12.97	627.02	18.75	11	13.01	608.97	32.93	11
13.48	633.28	26.50	8	13.51	613.78	18.35	8
13.92	641.80	9.42	4	14.07	630.68	15.21	6

B.4 Wind statistics for load measurements

In the comparison between measured and calculated loads that will be made in B.6 correct input data for the calculations are necessary. This especially applies to the values for turbulence and air density.

The turbulence value is known to be the dominant factor for fatigue loading, and although the two values are not entirely proportionally linked, the correct choice of turbulence level for the calculation approach is nevertheless critical to the result of comparison with measured data.

In Figure B-8 The measured turbulence is shown for the representative time series marked as 5 minutes average points. Shown also for each half m/s are the binning points for the average turbulence. However, the average value bins are not the turbulence value's that will be used as input to the load calculations.

Since the fatigue loads are calculated for an S/N curve value of m=8, and later on binned with the same value to correct for, as far as possible, the fact that the fatigue load should have been calculated for the complete connected time series and not chopped apart in pieces of it, it can be shown that binning the turbulence with the same m value, will give more correct results (the subject is further addressed in B.6.1). The spline curve, through the bin values for m=8 in Figure B-8 is in the load calculations used to determine the turbulence values for the used wind speeds. The measured air density and the binned values of the same are shown in Figure B-9 . The air density is proportional to the loading, and the binned values are used to determine the input value to the load calculations.

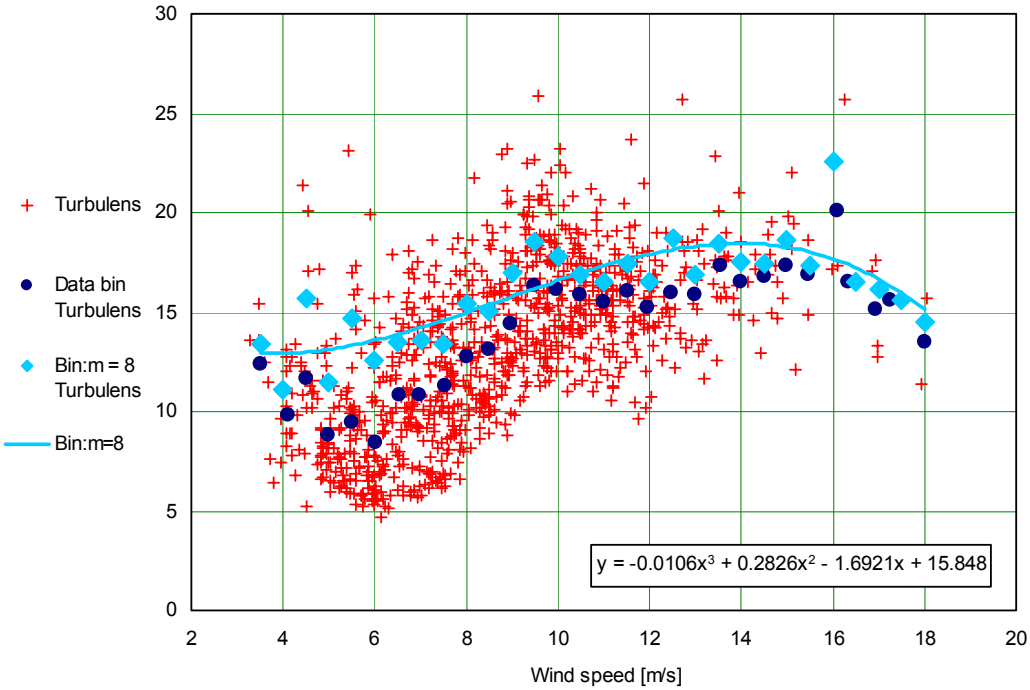

Figure B-8 Turbulence as function of wind speed shown as 5 minutes average points, average bin points (m=1), and bin points using an S/N-curve exponent of m=8.

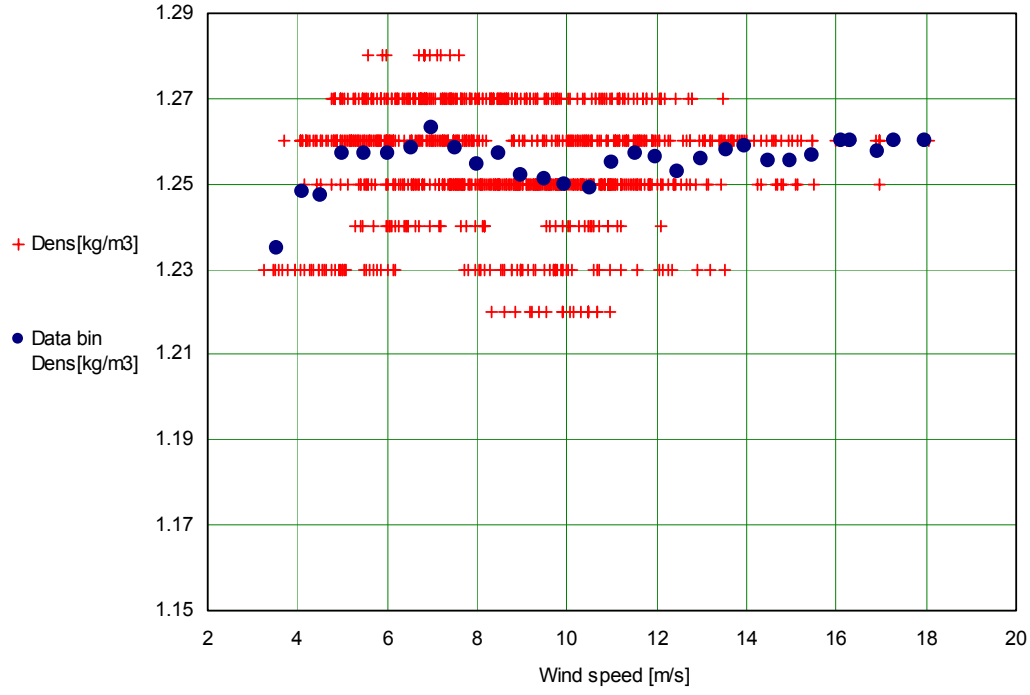

Figure B-9 Air density as function of wind speed shown as 5 minutes average points and average bin points (m=1).

B.5 Pitch statistics for load measurements

In Figure B-10 pitch angles are shown as function of the wind speed. Compared to Figure A-4 the figure shows the same, except for the identified offset. The measured pitch curve taking the offset into consideration is like the turbulence and air density used as input to the load calculations.

In order to have an ideal pitch curve, as outlined in [1], the curve profile should be monotonous decreasing in the wind speed region from 4 m/s to 12 m/s and then horizontal flat in the whole stall range. The obtained pitch curve does obviously not have this quality. The main reason for this was the discrepancy between the initial airfoil prediction and the actual airfoil characteristics. The actually obtained Cl_{max} was somewhat lower than anticipated, and it was therefore necessary to increase the pitch angle by up to 2 degrees more than anticipated at wind speeds around 12 m/s to get closer to the initially predicted power curve. A further discussion of this is addressed in chapter A.

A pitch characteristic as the one shown in Figure B-10 means that more pitch action is demanded to control the turbine power output, and an increased fatigue load on the pitch system is therefore unavoidable. However, it also means a higher number of situations where the pitch angle is incorrectly adjusted with respect to wind speed and resulting power level and from this it could be expected that the standard deviation of the power was higher than for the traditional blade where the pitch characteristic is much closer to the ideal case. Both the daily turbine operation and the measured loads showed that this was not the case, which in terms showed that the blades had a much less violent response to adjustment errors, and thus less load penalty.

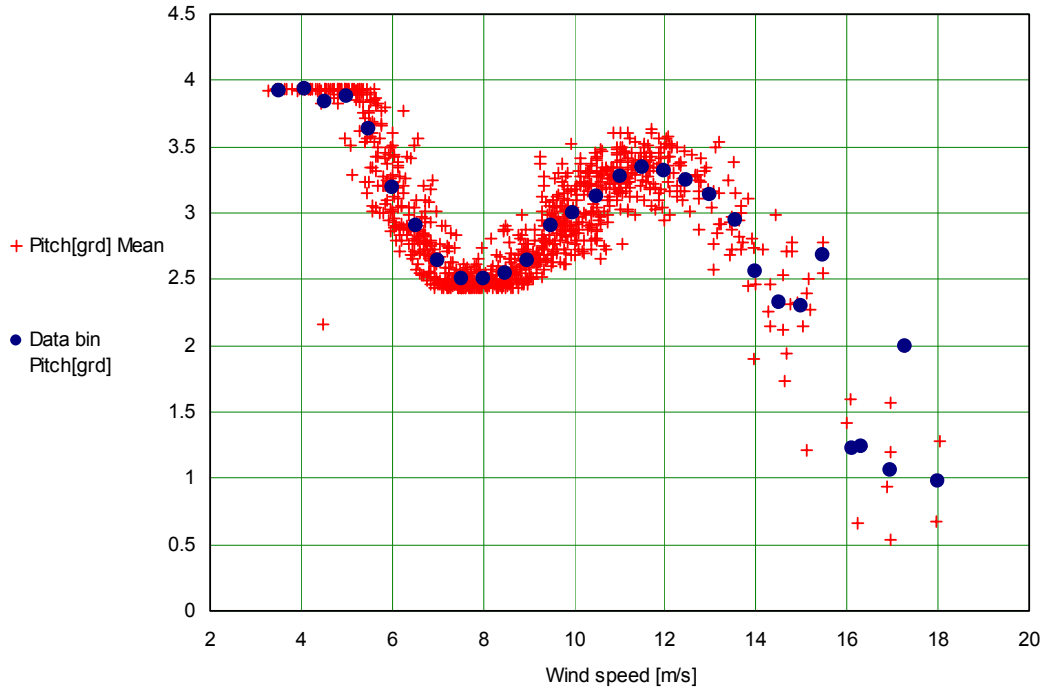

Figure B-10 Blade pitch angle as function of wind speed shown as 5 minutes average points and average bin points (m=1).

B.6 Loading analysis

B.6.1 Method description

For the loading analysis a representative time series sampled with 40 Hz, with duration of 142.5 hours and with a wind speed range from 3 m/s to 18 m/s was chosen. In the first processing of the series all situations where the turbine was stopping or starting, and situations with wake between either of the turbines or a turbine and the measuring mast (except for wind speeds above 14 m/s), was eliminated.

The resulting series was split into first a number of series of 5 minutes duration containing the loads that would later on be used for rain flow counting and second a file containing statistical values based on 5 minutes duration time. The load series was during the process passing a low-pass FIR filter, designed to the actual data, to clean up the data for noise that could influence the result of the analysis.

The reason for choosing a duration time of 5 minutes for the load series was that the aeroelastic load calculation program that would later on be used in the comparison was tailored for load series of 5 minutes duration.

The files containing the loads were saved in the format used by the aeroelastic code FLEX4, meaning that the same tools for load analysis can be used on the files, no matter if they are of simulation or measurement origin.

The next step in the analysis process was to use a rain flow counting procedure on each file, to calculate the fatigue damage loading. Since the load range's table resulting from the calculation on each file is not feasible to work with, a single number representing the load range table was established by recalculating the load range's into an equivalent load range R_{eq} using formula:

$$R_{Eq} := \left[\frac{\sum_{i=1}^{N_{levels}} (R_i)^m \cdot N_i}{N_{eq}} \right]^{\frac{1}{m}} \qquad \text{(B-1)}$$

Where R is the load range, N is the number of loads in this range and m describes the slope of the material S/N fatigue curve. Results were calculated for a number of different m values, but for the final comparison only m=8 were used. This value is a fair compromise between the m value for blades and the high-grade steel and cast iron structural elements in the hub.

The value N_{eq} is the reference load cycle number. It is very important in the comparison between measured and simulated data that this number is chosen the same, since the results will otherwise be scaled differently. In the present analysis N_{eq} is defined as if the load signal was alternating with a frequency of 1 Hz. This means that N_{eq} is 300 for the time series of 5 minutes duration (basing N_{eq} on a frequency instead of a finite number makes it in principle possible to compare time series of different duration).

Plotting the result of the calculations for all the time series results in a cloud of points. This is difficult to use directly because many different equivalent load levels are shown for each wind speed interval. To solve this, a binning of the point cloud is made. The binning is both made with m=1 resulting in an average value of the points, and with an m=8, which is the same value as used for the calculation of the equivalent load. Using m=8, it is taken into consideration that the equivalent loads with higher magnitude is more important, and that those loads would be dominating if the equivalent load were calculated from all the load series combined into one series. This also refers back to the choice of turbulences intensity (shown in Figure B-8) used in the load simulations.

In the following paragraphs B.6.2, B.6.3 and B.6.4 the measured and simulated loads are compared for the different load sensors. Besides comparison of the equivalent loads, the average loads (binned with m=1) are compared.

B.6.2 Power

With respect to the method description in B.6.1, the measured and calculated results are shown for the electrical power.

B.6.2.1 Load statistics

In Figure B-11 the measured statistical values for each 5 minutes file are plotted in terms of average, maximum and minimum extreme values. The maximum and minimum values are single instant short duration peak values in the file, and do in this manner represent the largest load range associated with the single file.

In Figure B-12 the standard deviation for the same files are shown. It is seen that the standard deviation is largest in the wind speed range from 9 m/s to 13 m/s. The simple type of control used in the test is operating on the measured nacelle wind speed and a pitch angle table as outlined in Figure B-10 , and since the pitch angle with the given pitch characteristics needs to be changed fairly much in the mentioned range, power overshoot resulting from lack of correspondence between wind speed and power is to be expected [12]. This is partly responsible for the shape of the standard deviation point cloud.

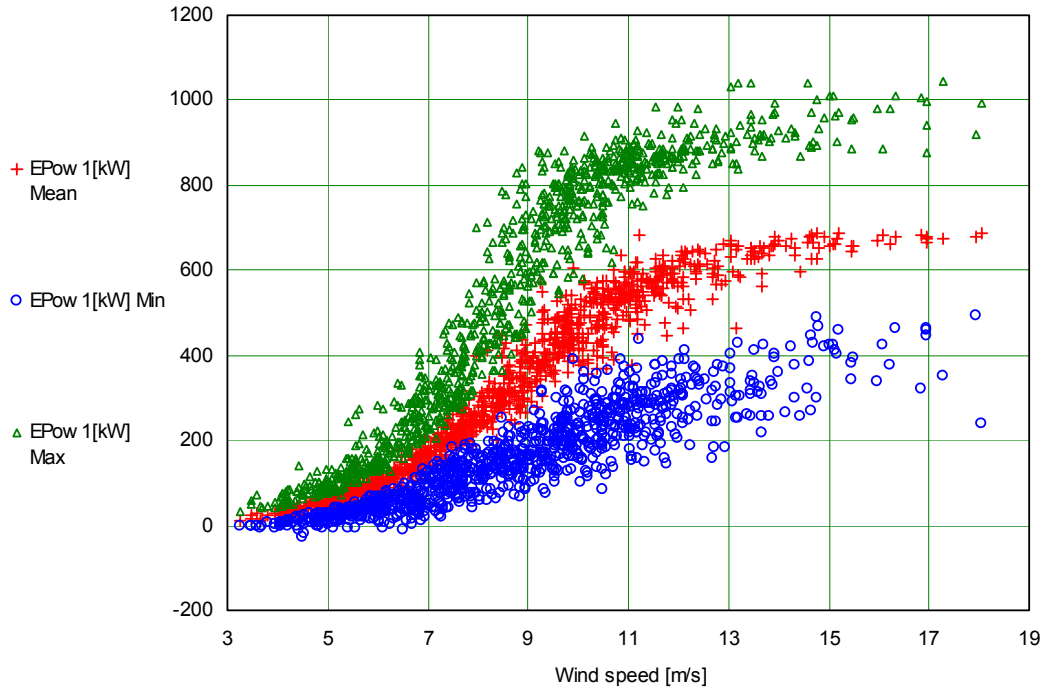

Figure B-11 Power curve shown as 5 minutes average points and maximum and minimum peak value within the 5 minutes.

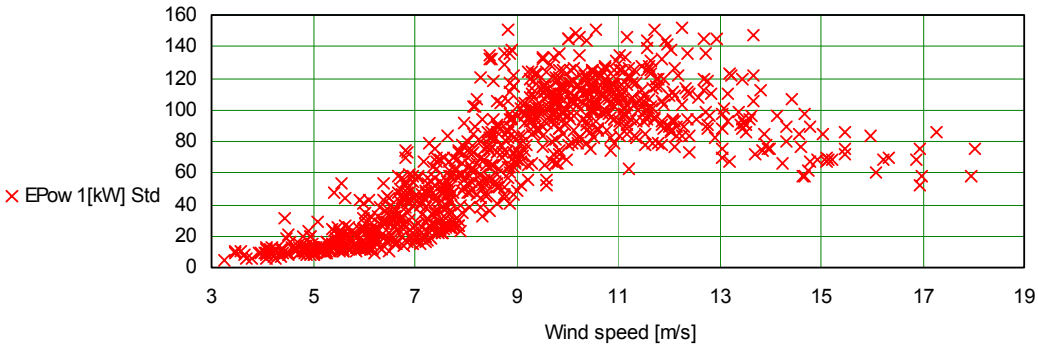

Figure B-12 Standard deviation of electrical power within the 5 minutes average.

In Figure B-13 the average values of the electrical power is binned to show the resulting power curve (not corrected to standard air density). The binned curve will later on be used for comparison with the simulated values.

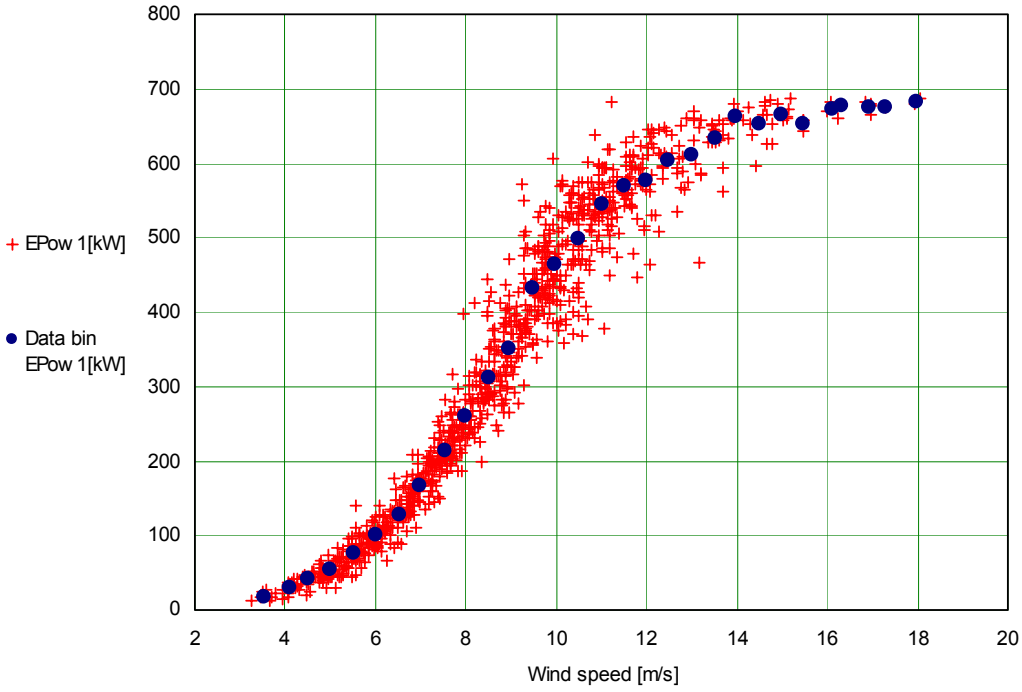

Figure B-13 Electrical power as function of wind speed shown as 5 minutes average points and average bin points (m=1).

B.6.2.2 Measured equivalent load

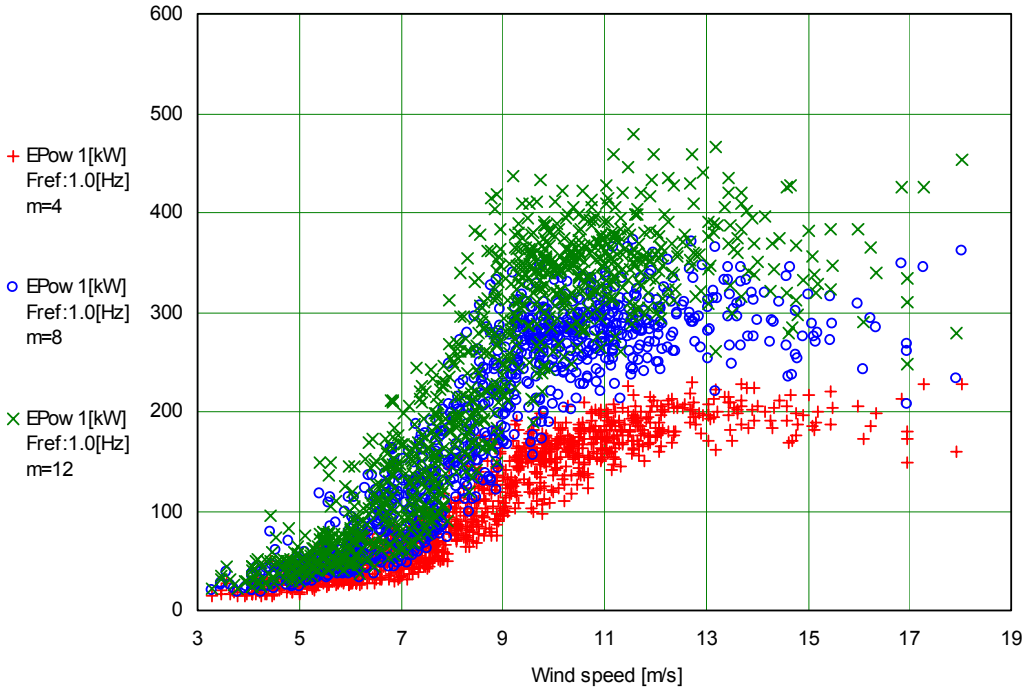

Figure B-14 Electrical power equivalent load as function of wind speed shown as 5 minutes points calculated for S/N-curve exponent values: m=4, m=8 and m=12, and for a total load cycle number derived from a 1 Hz load cycle frequency.

As by the method description in B.6.1 the equivalent load for the electrical power signal was calculated for S/N-curve exponent values m equal to 4, 8 and 12, for each of the 5 minutes files. The result is shown in Figure B-14. It is observed as expected, that the equivalent load value increases with increasing m value, and that the scatter of the points also increases because single large loads become more significant. However, it is seen as well that the shape of the point clouds are approximately the same for all m values, and that it therefore makes sense only to investigate one of those further.

Figure B-15 shows the point cloud for m=8. Further, binned values of the same are shown for two cases. In the first, the binning is made with the same exponent m=8, accounting for the fact that all the series within one wind speed bin interval ought to have been treated as one long undisrupted series. In the second, the binning is made with the same exponent m=1, which equals a simple averaging. In the further work, the m=8 binning will be used for comparison with simulated loads.

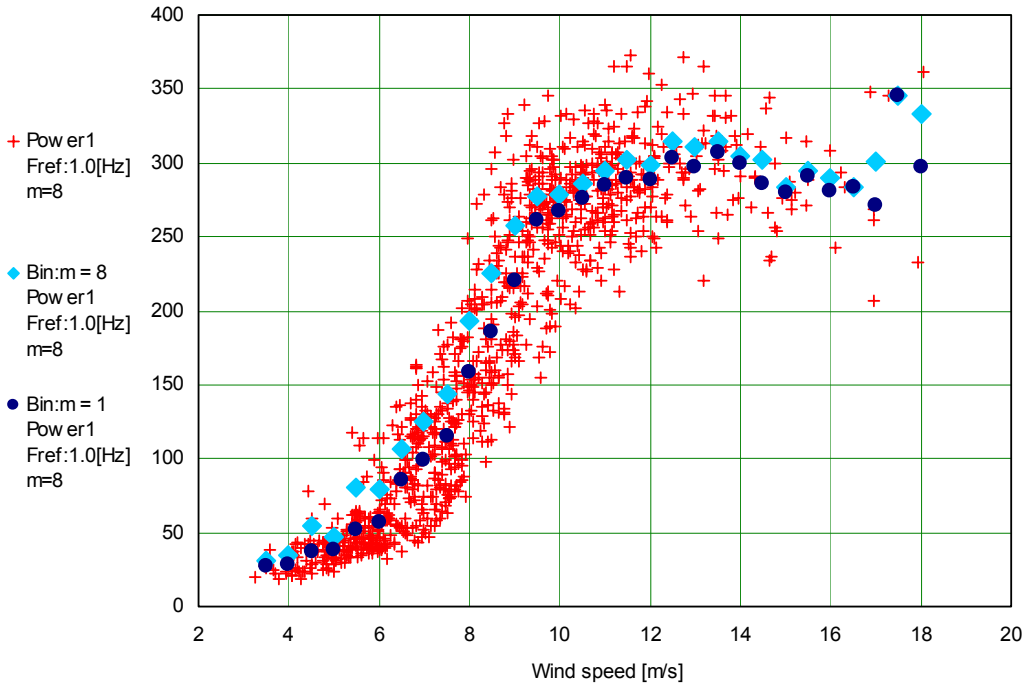

Figure B-15 Electrical power equivalent load as function of wind speed shown as 5 minutes points calculated for S/N-curve exponent value m=8 (1Hz load cycle frequency), and binned values for a bin exponent of m=1 (average value of points) and m=8.

B.6.2.3 Comparison of measured and calculated loads

The loads used for comparison with the measured loads were found using a simulation approach. With the blade data derived in A, simulations of the turbine were done in the aeroelastic code FLEX4. The parameters for the simulations were as far as possible adapted to the site conditions, i.e. by using the measured turbulence and air density as described in B.4. The simulations were then made in wind speed jumps of 2 m/s, in the range from 4 m/s to 18 m/s. For each wind speed used, two random seed parameters were chosen for the turbulence field. The results of the simulation were time series of 5 minutes duration that afterwards were processed through the exact same calculation procedures as used for the measured data.

In the first comparison shown in Figure B-16, average loads measured and simulated are compared. The result is seen to be fairly much off especially in the range between 8 and 14 m/s. This is a known problem with the simulation tool, and the same is found when simulations are made for the LM 21.0 P blade. It is however important to take this discrepancy into account when the overall comparisons between the blades are made B.7.2, where the produced energy is a factor of major importance. This calculation must show that the energy output from the two turbines is the same, in correspondence with the findings in B.3

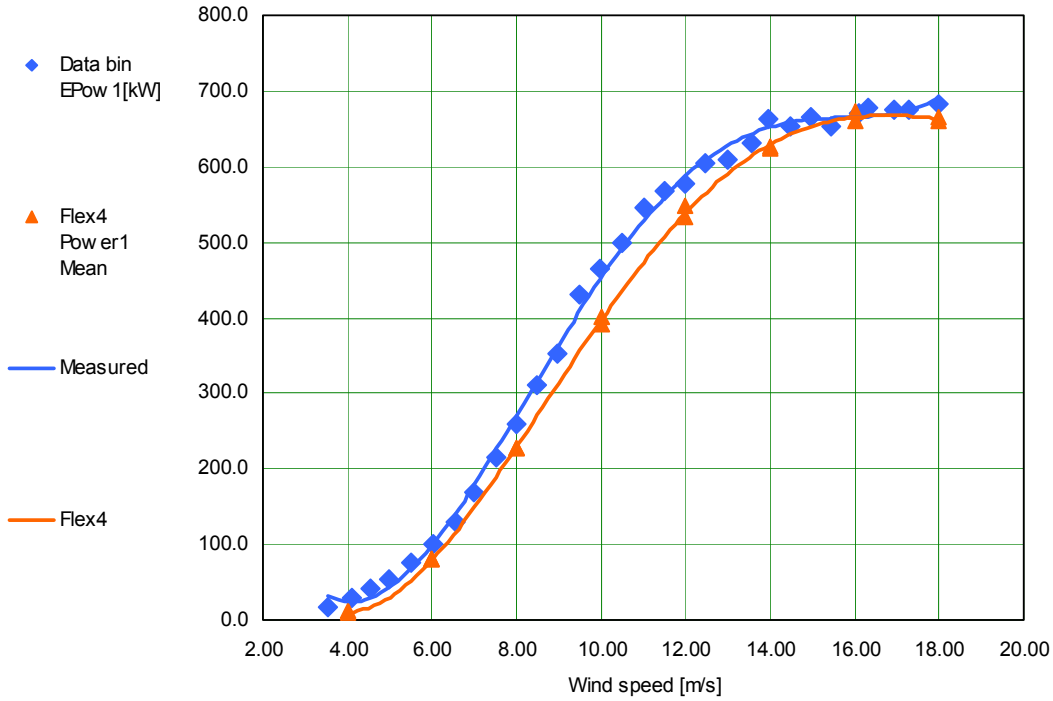

Figure B-16 Average electrical power as function of wind speed shown as bin values from measurements and points calculated with the Aero-elastic code FLEX4 under the same wind and air density conditions.

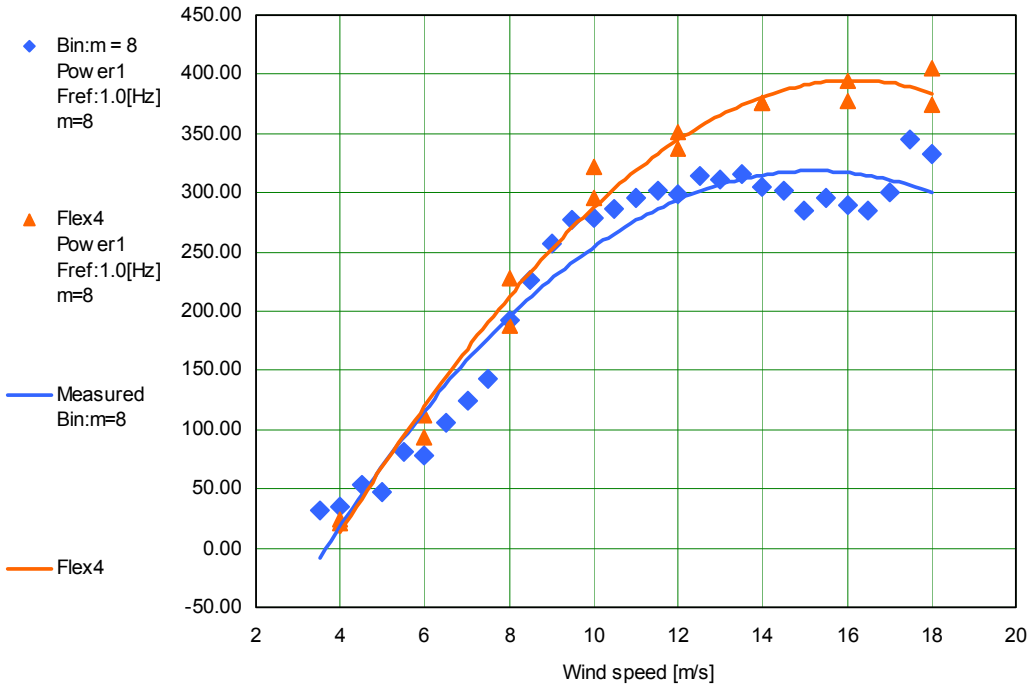

Figure B-17 Electrical power equivalent load as function of wind speed shown as bin values from measurements and points calculated with the Aero-elastic code FLEX4 under the same wind and air density conditions. Calculated and binned for S/N-curve exponent value m=8 (1Hz load cycle frequency).

The second and most important comparison between the equivalent loads is shown in Figure B-17. It is found that the measured and calculated loads are in agreement up to wind speeds of approximately 10 m/s. From this point up the calculated loads are overestimating the measurement fairly much. The reason for this has not been found, but it is assumed most likely to be due to a discrepancy in the wind model, or the wind model parameters. In the project it was not possible to conduct a full investigation of this, and

since the same wind model is used for both blades in the calculation comparison in B.7.2, it is not estimated to have a large impact on the final result evaluation.

B.6.3 Flapwise bending in radius 0.7 m

The procedure used for analyzing the measurement and calculation results for the flapwise bending in radius 0.7 m, is equal to the procedure used for the electrical power in B.6.2. The description in this part will therefore be limited to eventual comments to the figures.

B.6.3.1 Load statistics

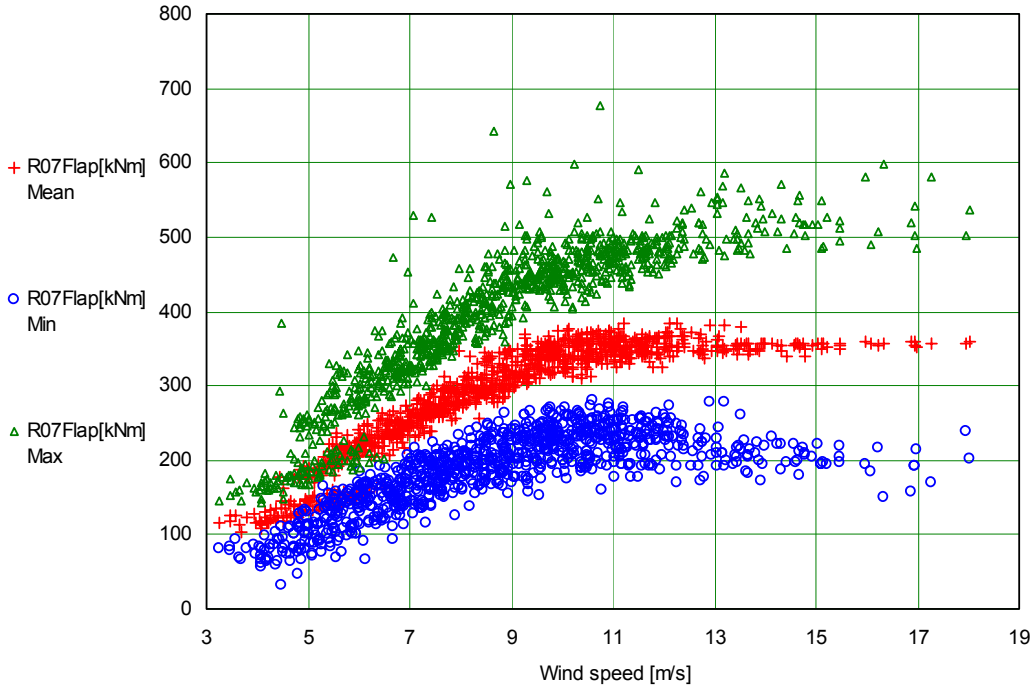

Figure B-18 Flapwise blade bending in radius 0.7 m from blade root shown as 5 minutes average points and maximum and minimum peak value within the 5 minutes.

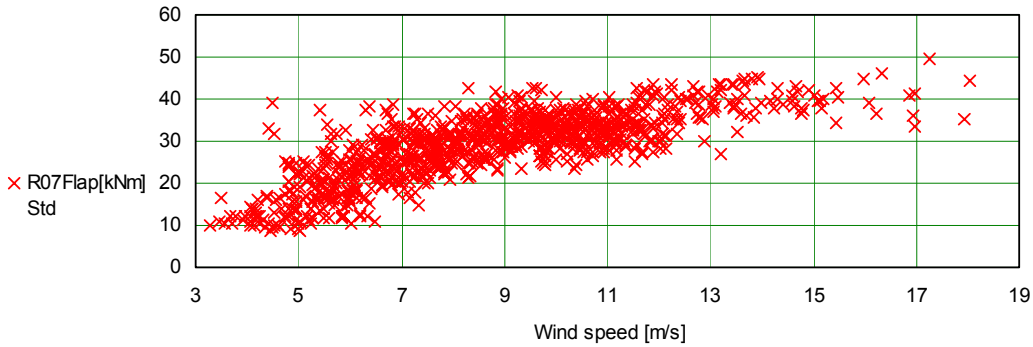

Figure B-19 Standard deviation of flapwise blade bending in radius 0.7 m from blade root within the 5 minutes average.

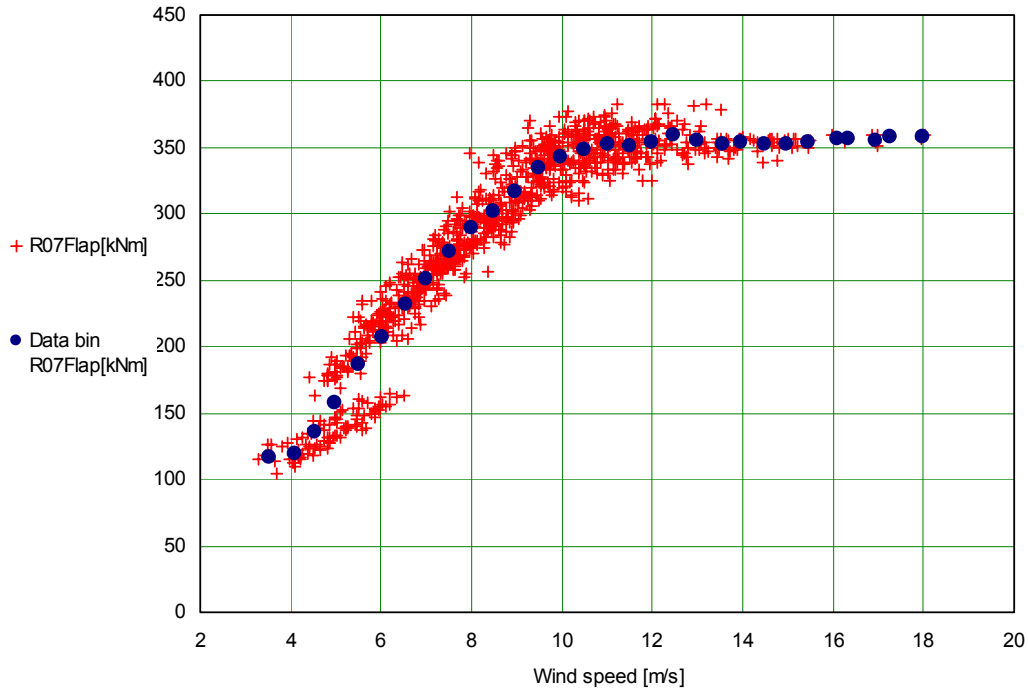

Figure B-20 Flapwise blade bending in radius 0.7 m from blade root as function of wind speed shown as 5 minutes average points and average bin points (m=1).

In Figure B-20 the Flapwise average points and the binned curve is shown. The two-stage generator operation is clearly observed between 5 m/s and 7 m/s. For the binned curve it was for convenience chosen to use the general average of the points, instead of splitting it in two curves.

B.6.3.2 Measured equivalent load

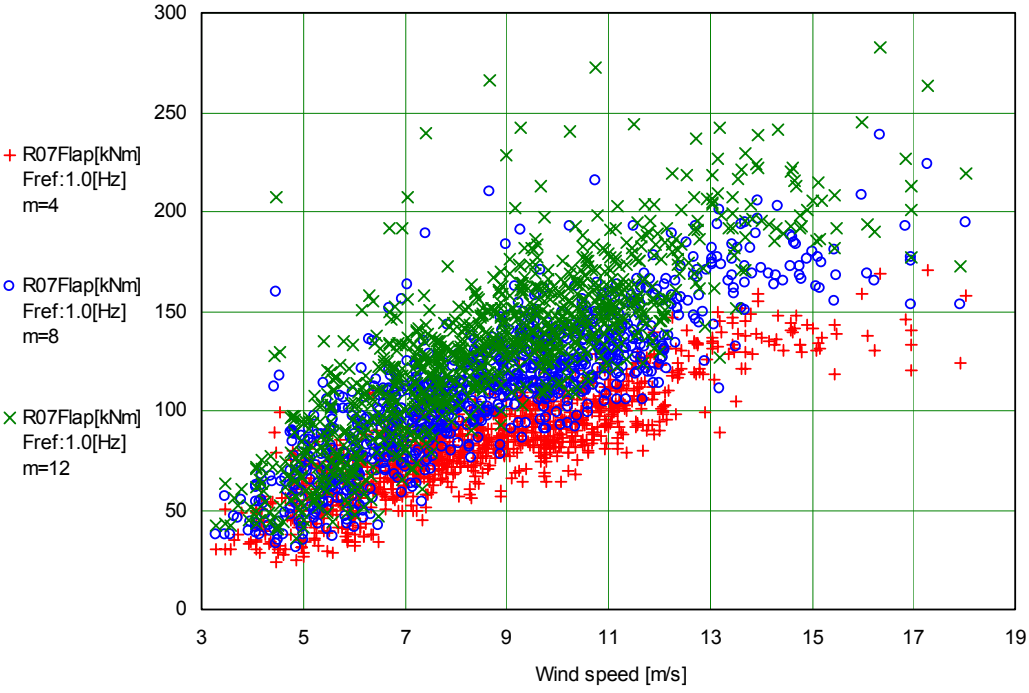

Figure B-21 Equivalent load of flapwise blade bending in radius 0.7 m from blade root as function of wind speed shown as 5 minutes points calculated for S/N-curve exponent values: m=4, m=8 and m=12, and for a total load cycle number derived from a 1 Hz load cycle frequency.

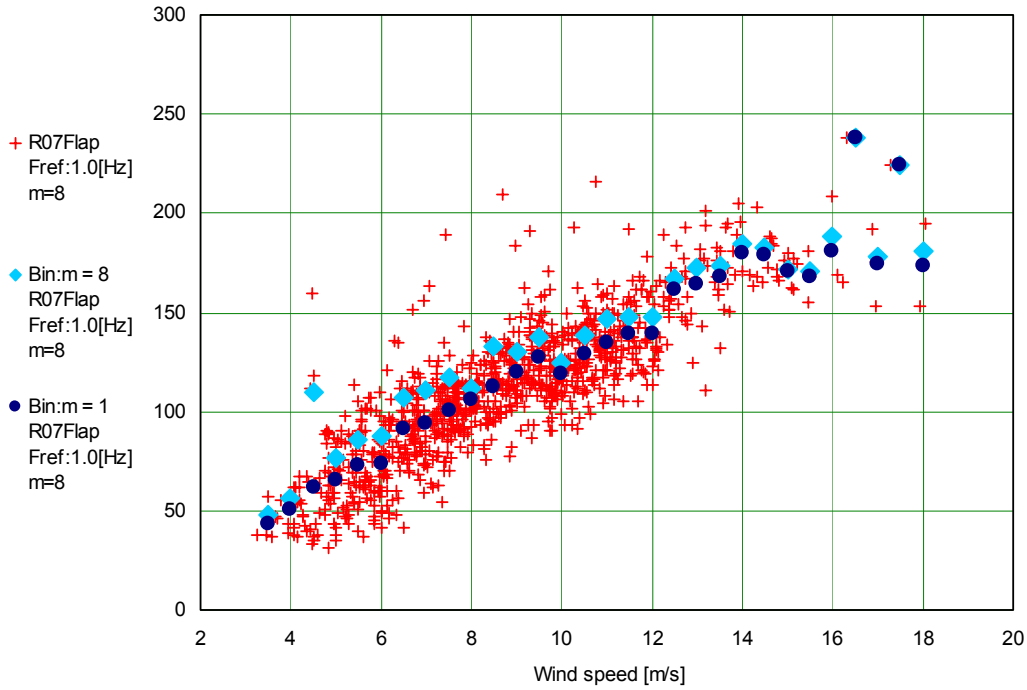

Figure B-22 Equivalent load of flapwise blade bending in radius 0.7 m from blade root as function of wind speed shown as 5 minutes points calculated for S/N-curve exponent value m=8 (1Hz load cycle frequency), and binned values for a bin exponent of m=1 (average value of points) and m=8.

B.6.3.3 Comparison of measured and calculated loads

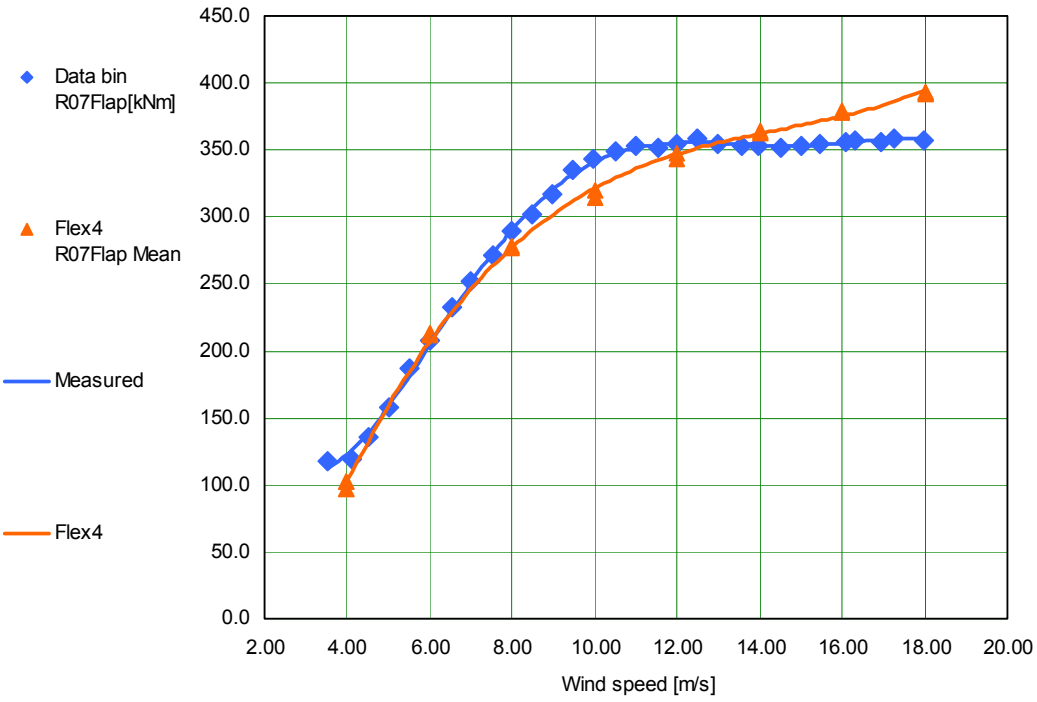

Figure B-23 Average flapwise blade bending in radius 0.7 m from blade root as function of wind speed shown as bin values from measurements and points calculated with the Aero-elastic code FLEX4 under the same wind and air density conditions.

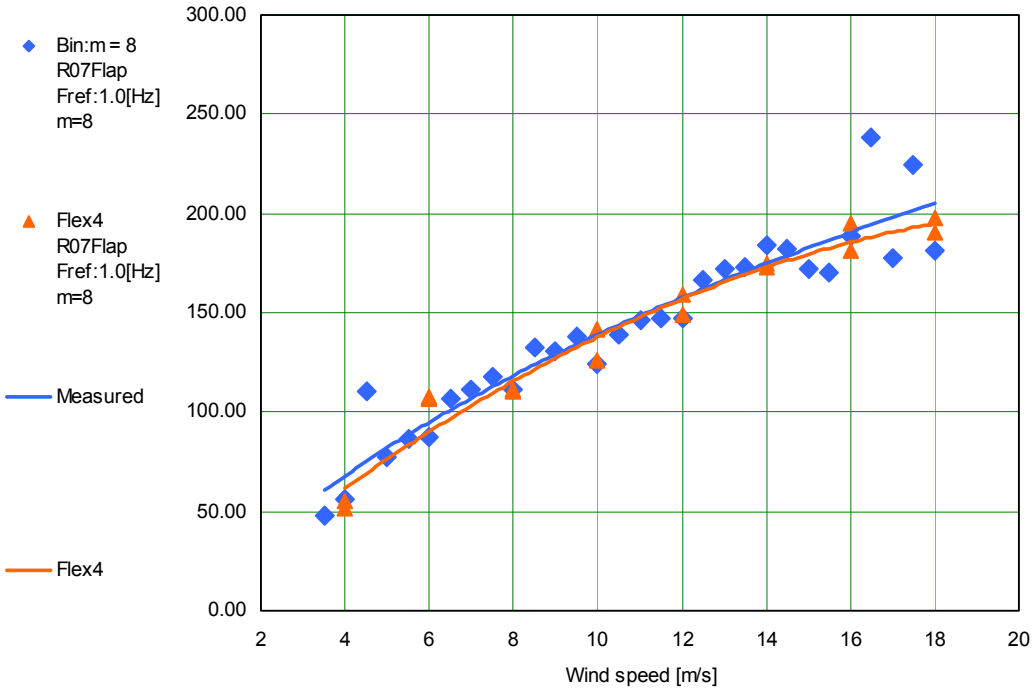

Figure B-24 Equivalent load of flapwise blade bending in radius 0.7 m from blade root as function of wind speed shown as bin values from measurements and points calculated with the Aero-elastic code FLEX4 under the same wind and air density conditions. Calculated and binned for S/N-curve exponent value m=8 (1Hz load cycle frequency).

In Figure B-23, average loads measured and simulated are compared. It is found that the result is fairly much in agreement except that the load is under predicted at 10 m/s and over predicted above 15 m/s. For the present investigation the deviation is acceptable.
The comparison between the equivalent loads is shown in Figure B-24. It is found that the measured and calculated loads are in excellent agreement in the whole wind speed range.

B.6.4 Flapwise bending in radius 4 m and edgewise bending

The measurements of flapwise bending in radius 4 m, was generally made to help deriving correct airfoil coefficients. During the analysis work, an uncertainty was however found in the calibration, and although the loads were analyzed like for the flapwise bending in radius 0.7 m, it was found that the uncertainty was to big and that the results would not provide additional information that was not already available. The analysis results from the flapwise bending in radius 4 m has therefore been omitted.

In the analysis of the measurements of the edgewise bending, it was found that one of the gauges was unstable, jumping between levels, and although the loads were analyzed it was decided that the results should not be used for the load comparison.

In lack of calibrated results and with the aim of conduction a load comparison (in B.7.2) by calculation, the load difference on the edgewise bending should be checked with the load difference on the power for the following reason: The main fatigue load contribution to edgewise blade root fatigue is the deterministic load resulting from the blade rotating in the gravitation field, which will be determined by the blade mass distribution. The remaining part of the fatigue load will result from stochastic loading, for which a part will be observed on the power signal as well. So, in the comparison between two blades, conditioned that the mass is the same, the difference in edgewise fatigue loading between the two blades will be reflected in the difference in the power loading. (If self-induced edgewise blade vibrations appears, this will most likely be the strongest source of edgewise fatigue loading. However, this has never been seen or recorded on any of the Norwin turbines).

B.7 Comparison of LM 21.0 P and LM 21.0 ASR blade performance

Having established in B.6 that the measured and calculated loads for the LM 21.0 ASR blade are in agreement makes it possible to compare the loads between the new and the traditional blades on a calculation basis. A direct measurement-to-measurement comparison would have been preferred, but measurements did not take place on the LM 21.0 P blades, and a calculation approach is therefore the only alternative. In the simulation of the wind turbine with different blades, the full power level regulation was used in order to include aspects of the blades regulation properties into the analysis.

The calculation of the LM 21.0 P blades is based on the airfoil data provided by LM Glasfiber.

In the comparison three blades are virtually looked at. The first is the original LM 21.0 P blade, the second is the new blade using the airfoil data as they were assumed to be after phase 1 of the project and the third is the new blade using the airfoil data derived in A.

The initial comparison is done on both mean load and equivalent load level and it is visualized through plots showing how the different blades behave.

For the final comparison it is not enough to look at the loads alone, since a load change could be balanced out by a likewise change in the energy production from the turbine, so to make an absolute evaluation it is necessary to compare the energy output to load ratio. This is done in B.7.2 where a single value for the equivalent fatigue load for each of the chosen load sensors are calculated for the 20 years operational loads in the wind speed range from 4 to 18 m/s. Similar, the energy production is calculated for the period. The final figures are expressed as percentage of load and energy production for the traditional LM 21.0 P blade.

B.7.1 Figures for statistics and equivalent loads

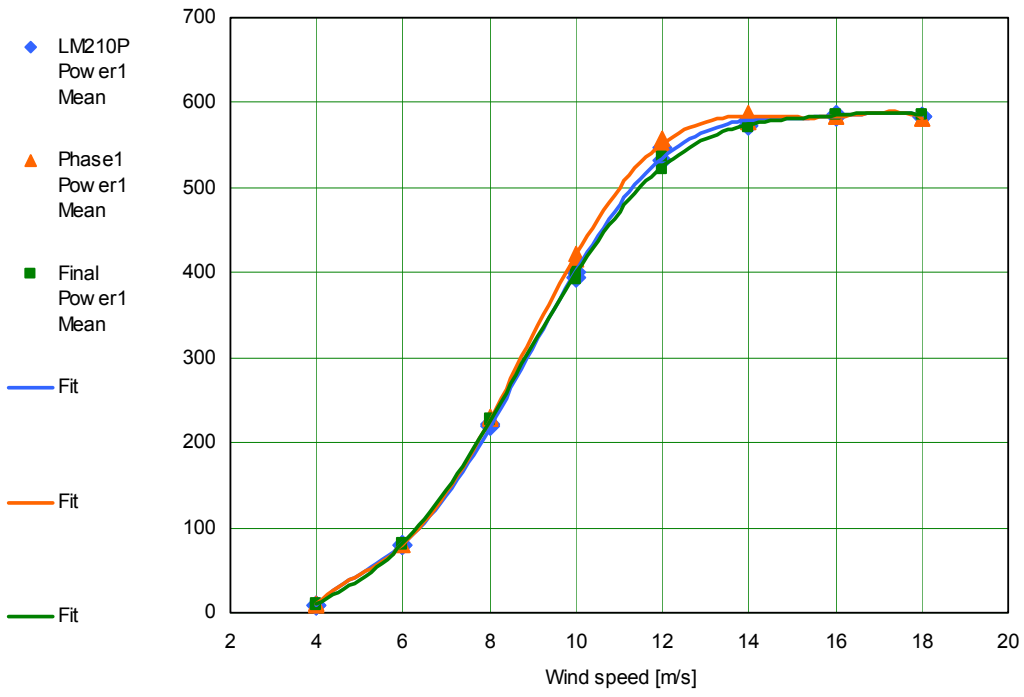

Figure B-25 Comparison of average electrical power calculated for the LM 21.0P blade, the LM21.0ASR blade with airfoil coefficients as estimated in project phase 1 (Phase1), and the LM21.0ASR blade with airfoil coefficients derived from the measurements (Final).

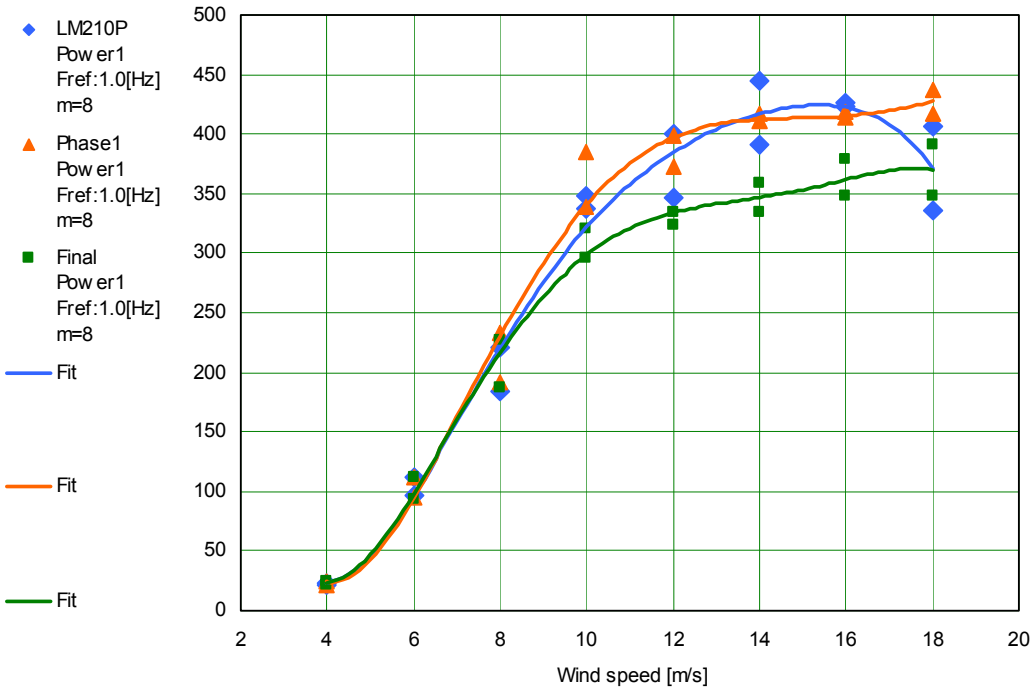

Figure B-26 Comparison of electrical power equivalent load calculated for the LM 21.0P blade, the LM21.0ASR blade with airfoil coefficients as estimated in project phase 1 (Phase1), and the LM21.0ASR blade with airfoil coefficients derived from the measurements (Final).

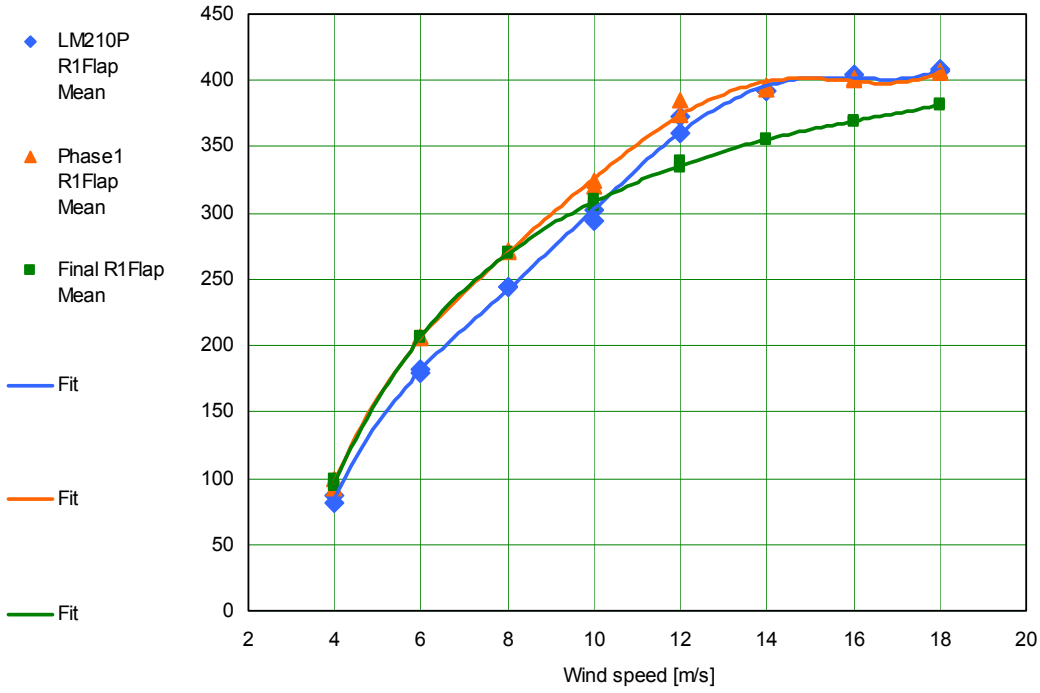

Figure B-27 Comparison of average flapwise blade bending in radius 1.0 m from blade root calculated for the LM 21.0P blade, the LM21.0ASR blade with airfoil coefficients as estimated in project phase 1 (Phase1), and the LM21.0ASR blade with airfoil coefficients derived from the measurements (Final).

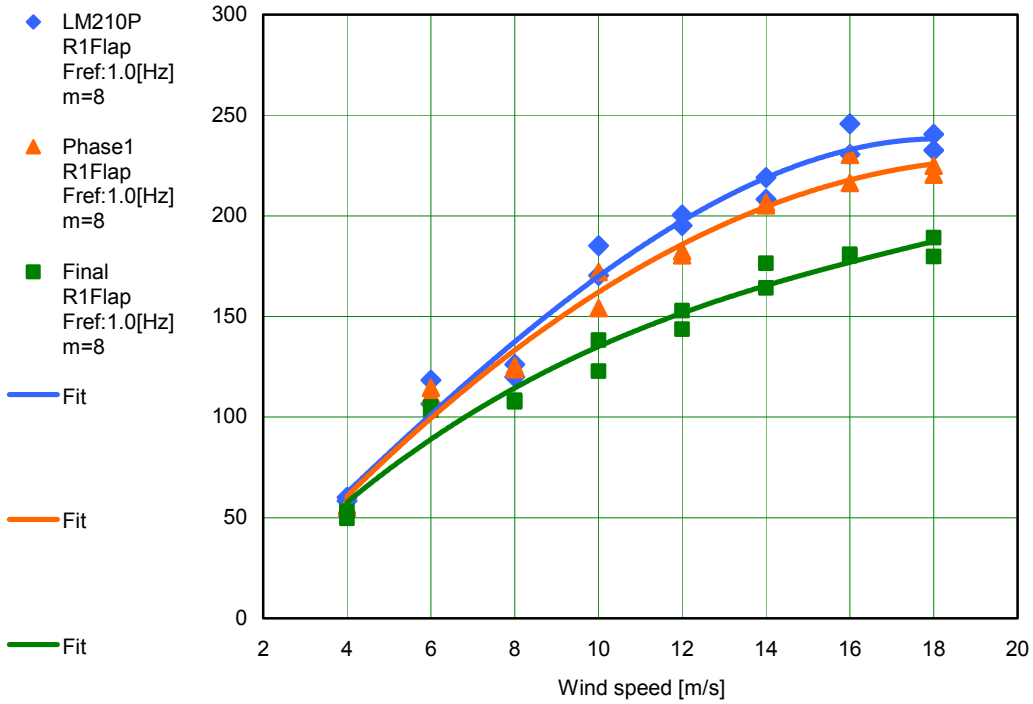

Figure B-28 Comparison of equivalent load for flapwise blade bending in radius 1.0 m from blade root calculated for the LM 21.0P blade, the LM21.0ASR blade with airfoil coefficients as estimated in project phase 1 (Phase1), and the LM21.0ASR blade with airfoil coefficients derived from the measurements (Final).

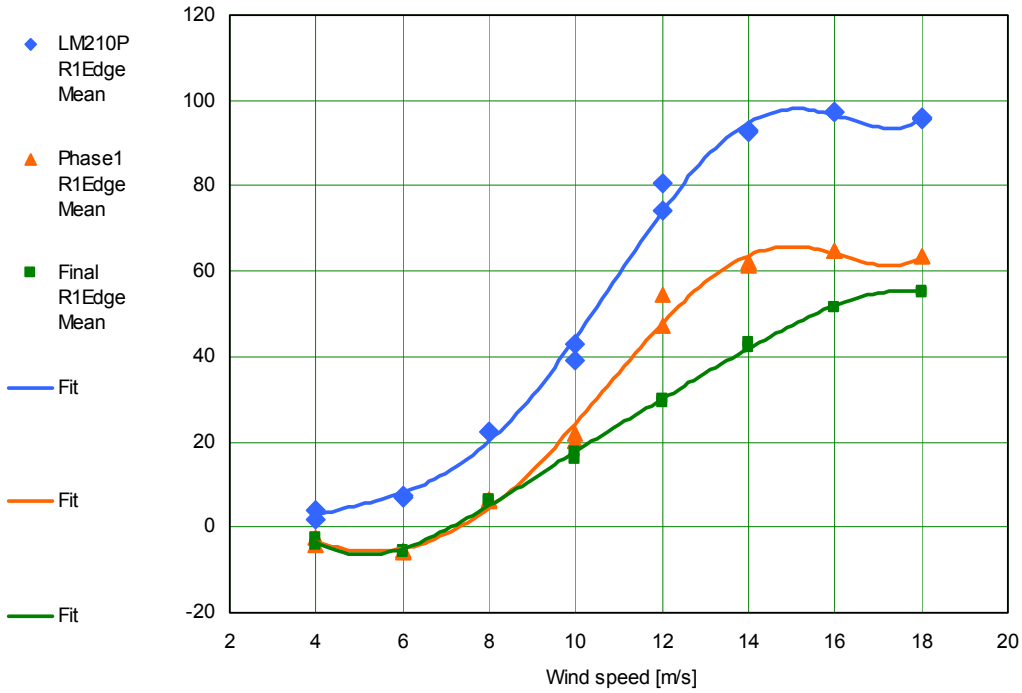

Figure B-29 Comparison of average edgewise blade bending in radius 1.0 m from blade root calculated for the LM 21.0P blade, the LM21.0ASR blade with airfoil coefficients as estimated in project phase 1 (Phase1), and the LM21.0ASR blade with airfoil coefficients derived from the measurements (Final).

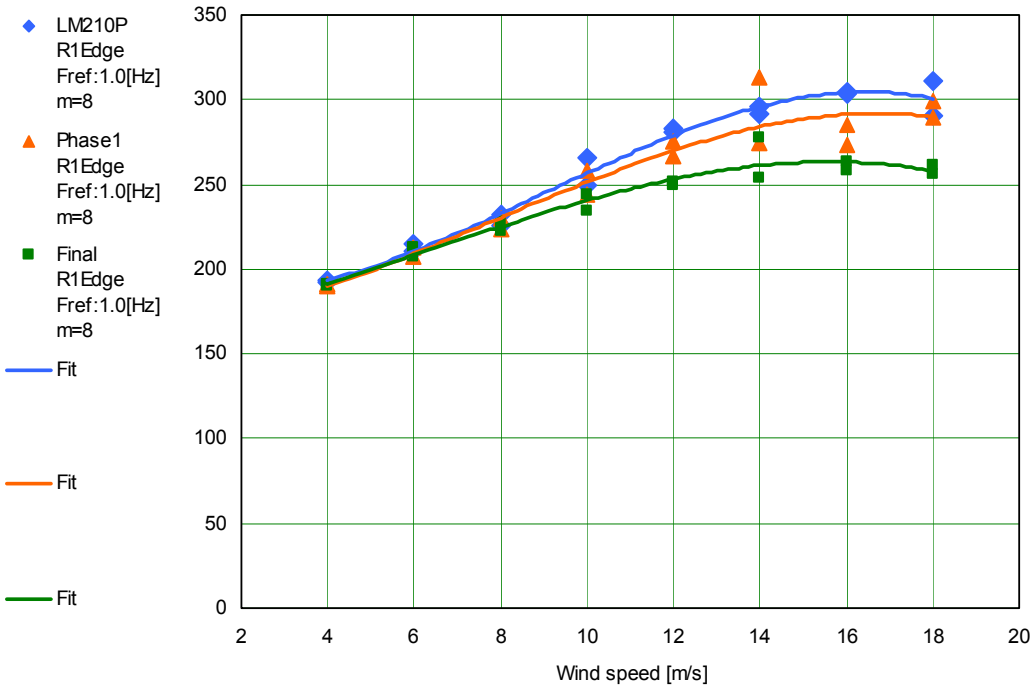

Figure B-30 Comparison of equivalent load for edgewise blade bending in radius 1.0 m from blade root calculated for the LM 21.0P blade, the LM21.0ASR blade with airfoil coefficients as estimated in project phase 1 (Phase1), and the LM21.0ASR blade with airfoil coefficients derived from the measurements (Final).

In Figure B-25 the average power is compare, and it is seen that the calculated power curves for the LM 21.0 P blade and the final LM 21.0 ASR blade, is very much in agreement with the findings in B.3.

Figure B-26 shows the equivalent loads for the electrical power and it is found that loading on the turbine with the final LM 21.0 ASR blade is significantly lower than both the LM 21.0 P blade and the ASR blade as predicted after phase 1.

The average flapwise bending comparison in Figure B-27 shows a little bit different characteristic for the blades. The average flapwise loading is normally not a very important figure, but a decrease in average loading at higher winds for the LM 21.0 ASR blade could have some impact in combination to the fatigue loading, because it is necessary to take the mean load into account in the fatigue strength calculation for composite materials. Further, a low average loading is a benefit for the blade control system.

Comparing the equivalent loads for the flapwise blade loading in Figure B-28 shows the most significant result in the analysis, since it is found that the final LM 21.0 ASR blade has a lower equivalent flapwise bending load in the whole wind speed range.

The average edgewise bending load, Figure B-29, and the equivalent edgewise bending load, Figure B-30, have some degree of uncertainty to it because the simulated results were not calibrated against measured data. However, as described in B.6.4, a comparison of the equivalent load results for the edgewise bending and the electrical power, will give a good indication about the validity of the observed differences between the blades. Comparing the curves shows that the difference between the LM 21.0 P and LM 21.0 ASR is in agreement.

B.7.2 Load and energy comparison

For the final comparison the energy output to load ratio of the turbine will be investigated. For each of the sensors: Electrical power (Power1), flapwise bending (R1Flap), edgewise bending (R1Edge) and power load density distribution equivalence (Power1ldd) a single value for the equivalent fatigue load is calculated for 20 years operational loads in the wind speed range from 4 to 18 m/s. Flapwise and edgewise bending is for convenience found in the radial blade station 1 meter from the blade root flange. The power load density distribution equivalence indicates the resulting load on the gearbox and is derived directly from the power, using the proportionality between power and main shaft torque.

The energy output during the 20 years of operational period is found in a similar manner.

In Table B-2 the result of the calculations are shown. To make the evaluation easier the derived values are expressed as percentage of load and energy production for the traditional LM 21.0 P blade. For the operational conditions in the period two types of terrain was looked at: A standard terrain type with a high average wind speed, and a terrain type 2 with a medium wind speed (the same as were used in [1]). As before a S/N curve slope of m=8 was used.

Table B-2 The calculated fatigue load and corresponding energy yield, for the turbine operating between 4 m/s and 18 m/s for a site with high average wind speed and a site with medium average wind speed. The result shown is a comparison between the LM 21.0 P blade and the LM 21.0 ASR blade with two different estimates of the airfoil coefficients (the estimate after Phase 1 of the project, and the final estimate based on the load assessments). The comparison is in percentage of the figures for the LM 21.0 P blade.

Total operating fatigue loads and energy yield
Base: N=10E7 m=8
Standard terrain type (High wind regime)
Comparison to LM21.0P in percentage

	LM210P Blade	Phase1 ASR blade	Final ASR blade
Power1	100	101	87
R1Flap	100	94	77
R1Edge	100	98	91
Power1ldd	100	104	99
Energy	100	103	100

Total operating fatigue loads and energy yield
Base: N=10E7 m=8
Terrain type 2 (Medium wind regime)
Comparison to LM21.0P in percentage

	LM210P Blade	Phase1 ASR blade	Final ASR blade
Power1	100	102	87
R1Flap	100	94	77
R1Edge	100	98	93
Power1ldd	100	104	98
Energy	100	103	100

Focusing on the traditional LM 21.0 P blade and the final LM 21.0 ASR blade, it is found that the energy yield from the blades are the same, which is supported by the practical findings on energy production from the turbines during the testing period. It was expected after end of project Phase 1 [1] that the new blades would produce approximately 3% more energy, but this showed not to be the case.

With equal energy production from the blades, the loads can be compared directly, and here a significant difference is found. After project Phase 1 [1] the loads were expected on average to increase slightly. Looking at the results for the Final LM 21.0 ASR blade is seen that the loads on the contrary are decreasing signifficantly. The blade loads are decreased with approximately 15% in average, and the power load (i.e. applied to main shaft torque) is decreased with approximately 13%. The power load density distribution equivalence is only slightly decreased which was expected since it links to the produced energy.

References

[1] Bak, C., Fuglsang, G., Sangill, O., Hansen, P., 1999, "Optimering af vinge til aktivt stallreguleret vindmølle." Risø-R-1132(DA), Risø National Laboratory, Roskilde, Denmark.

[2] Bak, C., Fuglsang, P., Sørensen, N.N., Madsen, H.Aa., Shen, W.Z., Sørensen, J.N., 1999, "Airfoil Characteristics for Wind Turbines." Risø-R-1065(EN), Risø National Laboratory, Roskilde, Denmark.

[3] Petersen, H., Benchmark test on power curve computations on wind turbines – a compendium, The Test Station for Windmills, Risø National Laboratory, Denmark (1986).

[4] Hansen, M.O.L., Øye, S., Generation of 2-D airfoil data for the BEM model, (In Danish) Project note, Institute of Energy Technology, Danish Technical University (1998).

[5] Øye, S., FLEX4 Simulation of Wind Turbine Dynamics, Proc. 28th Meeting of Experts, International Energy Agency, Annex XI, 1996, pp. 71-77.

[6] Fuglsang, P., 2002, "HAWTOPT User Manual Version 1.0a." Risø-I-1817(EN), Risø National Laboratory, Roskilde, Denmark, January 2002.

[7] Fuglsang, P., Madsen, H.A., Numerical Optimization of Wind turbine rotors, *Proc. European union Wind Energy Conference*, Göteborg, Sweden (1996)

[8] de Boor, C., A Practical Guide to Splines, Springer-Verlag. New York, 1978.

[9] Lading, P., 2002, "Målejournal K03 Ørsted 1" WEA Technology A/S, Roskilde, Denmark.

[10] Nielsen, T.E., 2002, "Analysis of Ørsted 1 and Ørsted 2." Internal project note.

[11] Fuglsang, P., Dahl, K.S., Antoniou, I., 1999, "Wind Tunnel Tests of the Risø-A1-18, Risø-A1-21 and Risø-A1-24 Airfoils." Risø-R-1112(EN), Risø National Laboratory, Roskilde, Denmark.

[12] Hansen R. S., Sangill O., Frandsen S., Lading P., Kristensen L., Miller G., 2001, "Laser Anemometry for Control and Performance Testing of Wind Turbines.", Publishable final report, The European Commission – Craft/Joule III.

Bibliographic Data Sheet **Risø-R-1374(EN)**

Title and authors

Design of a 21 m Blade with Risø-A1 Airfoils for Active Stall Controlled Wind Turbines

Peter Fuglsang, Ole Sangill, Peter Hansen

ISBN	ISSN
ISBN 87-550-3137-4; ISBN 87-550-3138-2(Internet)	ISSN 0106-2840
Department or group	Date
Wind Energy Department	12/20/2002
Groups own reg. number(s)	Project/contract No(s)

Sponsorship

The Danish Energy Agency under the contract, UVE-J.nr.51171/99-0028

Pages	Tables	Illustrations	References
57	13	55	12

Abstract (max. 2000 characters)

This is the final report, from the project, "Design of a Rotor/Airfoil Family for Active Stall-regulated Wind Turbines by Use of Multi-point Optimization". It describes the full scale testing of a 21 m wind turbine blade specially designed for active stall regulation. Design objectives were increased ratio of produced energy to turbine loads and more stable power control characteristics. Both were taken directly into account during the design of the blade using numerical optimization. The blade used the Risø-A1 airfoil family, which was specially designed for operation on wind turbine blades.

The new blade was designed to replace the LM 21.0P blade. A measurement campaign was carried out simultaneously on two identical adjacent wind turbines where one had the new blades and the other had LM 21.0P blades. Power and loads including blade section moments for the new blades were measured to assess the characteristics of the new blade. Airfoil characteristics, power curve and fatigue loads were derived on basis of the measurements.

Most of the design criteria for the new blade were met. The new blade had a reduced weight of 4% reducing blade cost compared with LM 21.0P. The measurements showed that the wind turbine with the new blades had the same energy production as the wind turbine with LM 21.0P blades but at the same time a 15% decrease in blade fatigue loads. However, the derived airfoil characteristics for the new blade were not in good agreement with the expected characteristics. The new blade was more sensitive to roughness and imperfections at the leading edge than initially foreseen and a high relative thickness in the tip region caused an unexpected drop in the maximum lift coefficient. This lead to discrepancies between the initial expected and actual pitch control characteristics.

It could be concluded that the new LM 21.0 ASR blade could replace the LM 21.0P leading to improved cost efficiency and that the Risø-A1 airfoils were well suited for active stall control. With the new established knowledge of the actual airfoil characteristics, a possible future blade design could be made also with improved power control characteristics.

Descriptors INIS/EDB

AIRFOILS; CONTROL; ELECTRIC POWER; OPTIMIZATION; TURBINE BLADES; WIND TURBINES